

Article

Experimental and Computational Fluid Dynamic—CFD Analysis Simulation of Heat Transfer Using Graphene Nanoplatelets GNP/Water in the Double Tube Heat Exchanger

Carlos C. X. S. Lima ¹, Alvaro A. V. Ochoa ^{1,2,*}, José A. P. da Costa ^{1,2}, Frederico D. de Menezes ^{1,2}, João V. P. Alves ², Julia M. G. A. Ferreira ², Clara C. A. Azevedo ¹, Paula S. A. Michima ¹, and Gustavo N. P. Leite ^{1,2}

¹ Department of Mechanical Engineering, Federal University of Pernambuco, Cidade Universitaria, 1235, Recife 50670-901, Brazil; carloslimac@gmail.com (C.C.X.S.L.); angelocosta@recife.ifpe.edu.br (J.A.P.d.C.); fredericomenezes@recife.ifpe.edu.br (F.D.d.M.); claracaroline_2@hotmail.com (C.C.A.A.); paula.michima@ufpe.br (P.S.A.M.); gustavonovaes@recife.ifpe.edu.br (G.N.P.L.)

² Department of Higher Education Courses (DACs), Federal Institute of Education, Science and Technology of Pernambuco, Av. Prof. Luiz Freire, 500, Recife 50740-545, Brazil; joaojoao.vitor3615@gmail.com (J.V.P.A.); juandraade77@gmail.com (J.M.G.A.F.)

* Correspondence: ochoaalvaro@recife.ifpe.edu.br; Tel.: +55-81-99976-4266

Abstract: This study investigates and compares the experimental heat transfer performance and simulation via computational fluid dynamics (CFD) of graphene nanoplatelets (GNP) and water nanofluids GNP/water in the double-tube-type heat exchanger (DTHE). Tests were conducted with water/water and GNP/water fluids, with the nanofluid for the hot-fluid circuit and water for the cold-fluid circuit, with counterflow direction, varying the nanofluid concentrations by weight (wt%) at 0.0125%, 0.025%, and 0.050%, the operating temperature at 50 and 60 °C, and Reynolds numbers between 2000–6000. The results showed that 0.025 wt% GNP presented better thermal performance, with a 28% increase in the temperature gain. The 0.025 wt% GNP had slightly better performance for the Nusselt number (Nu), and the 0.05 wt% GNP had a slightly better thermal effectiveness. The comparison between the experimental values showed good agreement with those calculated by empirical correlations and the CFD model, with maximum and minimum relative error values of 9% and 1%, respectively, when the Petukhov equation was used.

Keywords: double tube heat exchangers; heat transfer; nanofluids; graphene



Citation: Lima, C.C.X.S.; Ochoa, A.A.V.; da Costa, J.A.P.; de Menezes, F.D.; Alves, J.V.P.; Ferreira, J.M.G.A.; Azevedo, C.C.A.; Michima, P.S.A.; Leite, G.N.P. Experimental and Computational Fluid Dynamic—CFD Analysis Simulation of Heat Transfer Using Graphene Nanoplatelets GNP/Water in the Double Tube Heat Exchanger. *Processes* **2023**, *11*, 2735. <https://doi.org/10.3390/pr11092735>

Academic Editor: Udo Fritsching

Received: 21 August 2023

Revised: 5 September 2023

Accepted: 6 September 2023

Published: 13 September 2023



Copyright: © 2023 by the authors. Licensee MDPI, Basel, Switzerland. This article is an open access article distributed under the terms and conditions of the Creative Commons Attribution (CC BY) license (<https://creativecommons.org/licenses/by/4.0/>).

1. Introduction

Given the current rise in global energy consumption, the generation and use of energy have become a pressing issue worldwide. The high costs and growing use of fossil fuels have raised concerns about the scarcity of these nonrenewable resources. As a result, large industries have invested heavily in developing high-performance systems and devices that can optimize the use of available resources to reduce energy consumption and improve efficiency [1]. Energy savings can be achieved through efficient use and by avoiding damage to the environment and depletion of resources in the long term. Some ways to reduce energy consumption include conversion, conservation, and energy recovery [2]. Heat exchangers and/or recuperators are devices that have been helping to optimize the use of inputs in different industrial processes, such as chemical, petrochemical, food, power plants, pharmaceutical, environmental engineering, refrigeration, and air conditioning, among other applications [3].

Scientists, engineers, and researchers have been attempting for decades to improve the heat transfer efficiency of heat exchangers [4]. There are different heat exchanger configurations, such as shell and tube, plate, coil, and double tube, among others, which can be used in various heat transfer applications that require specific conditions and

specifications for effective heat transmission. However, these types of equipment can present a high investment cost, which has led to the search for optimization methods, as seen in the literature [5]. Models and optimization tools based on energy and financial balances have been analyzed to improve the thermal–hydraulic performance [6–9].

Conventional heat transfer fluids have low transfer properties, which has led to an increasing demand for developing fluids with better heat transfer performance [6,10]. One solution is to incorporate suspended solid particles, called nanoparticles, of nanometric size within the range 1–100 nm, into conventional fluids to increase their energy performance. These new fluid configurations are called nanofluids (NFs) [11].

NFs are considered as a new class of engineering fluids and are used as new heat transfer media, presenting a higher absorption capacity [12]. The trough thermal processes of nanofluids in heat exchangers have several advantages, such as improved thermal conductivity stability, as shown in the literature. Consisting of the dispersion of nanomaterials in a base fluid, such as ethylene glycol, water, oils, or even ionic liquids, the thermal properties (e.g., thermal conductivity) of nanomaterials are better than the base fluid [13]. They also present advantages in the application of heat exchangers not only because of their thermophysical properties but also in the geometric parameters of the heat exchange equipment and the working conditions. It can reduce the pressure drop and volume of the heat exchangers when compared with the base fluids, and increase the effectiveness of the heat exchanger regarding the nanofluid used [14,15], hence, leading to low energy consumption and low economic cost [16,17].

Furthermore, due to their higher thermal conductivity compared to base fluids [18], and high cooling potential, NFs provide excellent thermal performance in heat exchangers used in thermal energy transport applications, promising higher heat absorption and heat transport capacity, as shown in the literature [8,19].

The use of NFs in heat exchangers has gained attention in research worldwide due to the solid particles in suspensions contributing to a greater and better heat exchange between the fluids in the exchangers. The behavior of double-tube-type heat exchangers (DHTE) using nanofluids has been the subject of several studies, as shown in the literature [20].

Moghadam et al. [21] performed an analysis and optimization of the thermohydraulic system in a DTHE, with Fe_3O_4 /water nanofluid and longitudinal for turbulent flow, evaluating diameter ratio (DR) and performance ratio (PEC) parameters, with each parameter being optimized by using the single objective function (SOF) and multiobjective function (MOF) methods. The results showed that DR exerts the most and AR the least impact on the performance of the analyzed heat exchangers. Nonetheless, the addition of 0.03% nanoparticles in water leads to a 6.2% decrease in entropy generation number and a 13% increase in irreversibility distribution ratio.

Analyzing the same heat exchanger configuration (DTHE) and using a CuO/water nanofluid as the coolant, Khosravi et al. [22] numerically investigated the heat transfer characteristics with different inner tube geometries. The results showed that the convective heat transfer coefficient increased by up to 22% in the four-finned tube compared to the smooth tube, and increased by 17% in the eight-finned tube with air and nanofluid as working fluid as compared to the four-finned tube.

Testing the thermal and hydraulic performance of using nanofluid in DTHE heat exchangers, Raei et al. [23] analyzed the pressure drop decrease and heat transfer performance using a drag reduction agent (surfactant) in Al_2O_3 /water nanofluid at different concentrations in a finned tube heat exchanger. It was found that the nanofluid with a weight concentration of 0.2% (without the drag reducing agent) increased the heat transfer by 20% with a penalty of 5% increase in pressure drop. On the other hand, with a surfactant concentration of 100 ppm and the highest concentration of nanoparticles (0.2% by weight), there was an overall increase in heat transfer coefficient at 17.2% and a reduction in friction factor at 4.8% compared to water.

Bashtani and Esfahani [24] numerically studied a DTHE with a single and a corrugated tube, assuming three different wave amplitudes and water flow in parallel, where it was

determined that the Nusselt number for the DTHE with corrugation was 1.75 times that of the single tube DTHE exchanger. Wijayanta et al. [25] performed a study with double delta-wing ribbon inserts in a DTHE, using water as the working fluid and analyzing the heat transfer characteristics, varying the Reynolds number from 5300 to 14,500, applying wing widths at 0.31, 0.47, and 0.63, and using CuO/water nanofluid as the cooling fluid. The Nusselt number, thermal performance factor, and friction factor of the heat exchanger increased as the proportion of the width of the double-delta wing tapes increased.

It is known that an important aspect to consider in DTHE heat transfer is increasing the convective coefficient. In this regard, when analyzing the incorporation of Al₂O₃/water nanofluid into a counterflow DTHE, Bahmani et al. [26] found that increasing the volume fraction of the nanoparticles or the Reynolds number leads to an increase in the Nusselt number and the convective heat transfer coefficient. The maximum thermal efficiency and average Nusselt number increased by 30% and 32.7%, respectively, compared to water.

Another important factor that has been investigated is the pressure drop, in this case, the friction factor that the introduction of nanoparticles into the working fluid can cause, as shown in Kumar et al. [8]. Heeraman et al. [27] reported an experimental study targeting heat transfer and friction factor using a double tube heat exchanger. Concavity grooves were placed to increase heat transfer and slightly reduce pressure drop. The effect of using tubes with different corrugation diameters on heat transfer and friction factor properties was discussed. The result showed that modifications of corrugated tubes provide an excellent and economical alternative to improve heat transformation in heat exchangers. It was found that using water, lower operating parameters, and a higher Reynolds (Re) number resulted in better thermal conditions. The new geometry caused a lower pressure drop despite its higher convective heat transfer coefficient. The results also showed that increasing the nanofluid concentration and Re number increases pressure drop.

In an experimental analysis on a DTHE, Heeraman et al. [27] tested friction factor and effectiveness using Fe₃O₄/water nanofluid for the hot circuit and water for the cold circuit in different concentrations (0.005%, 0.010%, 0.030%, and 0.060%, by weight), with longitudinal tab inserts with aspect ratios 1, 2, and 4, and a wide Reynolds number range (15,000–30,000). The results showed that the heat transfer process increased with nanoparticle concentration and Reynolds number. However, this increase was further intensified with the reduction in aspect ratio values for the longitudinal insertions of the strip.

Wu et al. [28] experimentally investigated the pressure drop and convective heat transfer characteristic using Al₂O₃/water nanofluid in a helical DTHE, varying nanofluid concentrations (0.78% to 7.04%, by weight) and applying laminar and turbulent flows. The use of nanofluid showed remarkably similar behavior (in pressure drop and performance) to that in tubes with helical coils.

Nagaraju et al. [29] presented a new alternative elliptical tube manufactured from graphene nanofluids to improve the convection heat transfer characteristics. The work was divided into two parts, the first part aiming at the experimental configuration using circular tubes and the second part through developing a CFD model using the finite volume method.

It was found that placing the oval tube in an alternate direction tends to improve the secondary flow region with a high eddy, leading to a lower thickness in the thermal boundary layer. On the other hand, the Nusselt number increases by an average of 10%, 29%, and 39% for graphene nanofluids prepared using weight concentrations of 0.05%, 0.1%, and 0.2%, respectively, considering 80 °C temperature. In the same context, however, a performance study was carried out considering a microchannel exchanger using nanofluids with graphene quantum dots [30]. The graphene quantum dot nanofluid considered had 0–0.5% concentrations and Reynolds numbers ranging from 50 to 200 (hot fluid) and Reynolds numbers from 100 (cold fluid). The study had a 3D numerical approach based on the finite volume technique. The results revealed that with Reynolds numbers of 50 and 100, using the nanofluid tends to significantly improve the heat transfer rate, with a slight increase in the pressure drop. However, for Reynolds numbers 150 and 200, using

the nanofluid imposes a significant pressure drop on the system. These results indicate that using the graphene quantum dot nanofluid allows for excellent performance between Reynolds numbers of 50 and 100. For Reynolds numbers 150 and 200, the use of the nanofluid is limited by the significant increase in the pressure drop.

Elbadawy et al. [19] presented a numerical study on fluid and heat transfer characteristics considering different nanofluids ($\text{Al}_2\text{O}_3\text{-H}_2\text{O}$, $\text{TiO}_2\text{-H}_2\text{O}$, and $\text{SiO}_2\text{-H}_2\text{O}$), as well as different microchannel heat sink configurations (rectangular, triangular, trapezoidal, and circular). The average heat transfer coefficient h and the pressure drop Δp quantify the fluid flow and heat transfer characteristics in each microchannel configuration on the heat transfer (MCHS) configuration and for each nanoparticle concentration. It was found that the best heat transfer coefficient was obtained with $\text{Al}_2\text{O}_3\text{-H}_2\text{O}$ compared to other types of nanoparticles and pure water. In addition, the best geometric configuration for the system was with the triangular-type microchannel heat sink, with a higher pressure drop due to the smaller hydraulic diameter.

The literature review showed that studies have analyzed other energy performance parameters in double-tube-type heat exchangers from the experimental or numerical points of view, seeking promising and innovative nanofluids based on graphene nanoparticles (GNP). However, no specific conclusions have been made on the effectiveness, energy performance, and hydrodynamic behavior of the system. Therefore, the aim of this work is to investigate and compare the heat transfer performance of GNP/water nanofluids in the double-tube-type heat exchanger (DTHE), through experimental/numerical analysis via CFD. The study considers different fluids, such as water/water and GNP/water, and a counterflow heat exchanger. A sensitivity analysis was performed to test the energy performance of the fluids with or without nanofluid in the heat exchanger, and varying the nanofluid concentrations, operating temperature, and at different Reynolds numbers.

The significance and novelty of the study presented is its use of nanofluid, specifically graphene as nanoparticles, which reflects a new component that could help design smaller heat exchangers, lower-cost devices, greater efficiencies, and even less head loss along the system by adding a sufficient volume of nanofluid at a specific concentration to enrich the heat and mass transfer process for industrial applications.

2. Nanofluids Preparation and Characterization

There are several methods described in the literature for development and improvement of GNP nanofluids production. Depending on the quality of the desired product and the intended application, one or more methods can be used [31,32]. Two basic methods are used to synthesize nanofluids: the one-step and the two-step methods. In the one-step method, the nanofluid is prepared simultaneously by producing and dispersing nanoparticles in the liquid base, which includes the chemical deposition methods of liquids and vapors. It includes only one step: drying, storage, transport, and stable dispersion of the nanoparticles to minimize their agglomeration [33]. However, this method is not feasible for large-scale nanofluids due to its high production cost. The two-step method was the one developed for the fabrication of the GNP nanofluids used in this research. It is the most widely used method to synthesize nanofluids, and it consists of synthesizing the nanoparticles in the form of ultrafine dry powder, which is subsequently dispersed in the base fluid by physical processes (ultrasound, magnetic stirrer, and homogenizer) and by using a dispersion agent to avoid nanoparticle agglomeration [33–36].

The fabrication of GNP nanofluids was performed by electrochemical exfoliation, as described by Hernandez et al. [37]. Initially, pre-exfoliation occurred, where the graphite bar was placed in a three-way flask with 100 mL of sodium hydroxide solution, connected to an ICEL PS-1500 Source with the power at 10.0 V for 1 h at a constant voltage. Subsequently, the electrodes were transferred to a 0.5 M sulfuric acid solution under a voltage of 7.5 V for 24 h. At the end of exfoliation, the precipitate is filtered with a paper filter and washed with distilled water, ethanol, and propanol for further removal of impurities and pH regulation. The exfoliated graphite in powder form was placed in an oven to dry at 60 °C for 24 h. It is

then ground and dissolved in 500 mL of distilled water with the addition of the surfactant Sodium Lauryl Ether Sulfate at different concentrations and placed in a Bandelin ultrasonic homogenizer for 3 h to finish the exfoliation of graphite particles to produce the GNPs. At the end of the homogenization, the GNP nanofluid was dissolved in 7 L of distilled water so that it could be used in the heat exchanger tests.

Figure 1 presents the scanning electron microscopy (SEM) image of the morphology and structure of the GNPs, made from the graphite bar. Its analysis was characterized using a Tescan MIRA3 SEM. The SEM image indicates the formation of sheet-shaped graphene nanolayers, a material formed by sheets [38] that are interconnected and have roughness on their surface. It can be observed Figure 1a that the ordered stacking of at least four graphene layers in a nanoplatelet, in a two-dimensional structure, confirming the multilayered nature of analyzed graphene sheets, as indicated by the arrow. In Figure 1b, note its rough surface, which can be compared with results found in the literature [39,40].

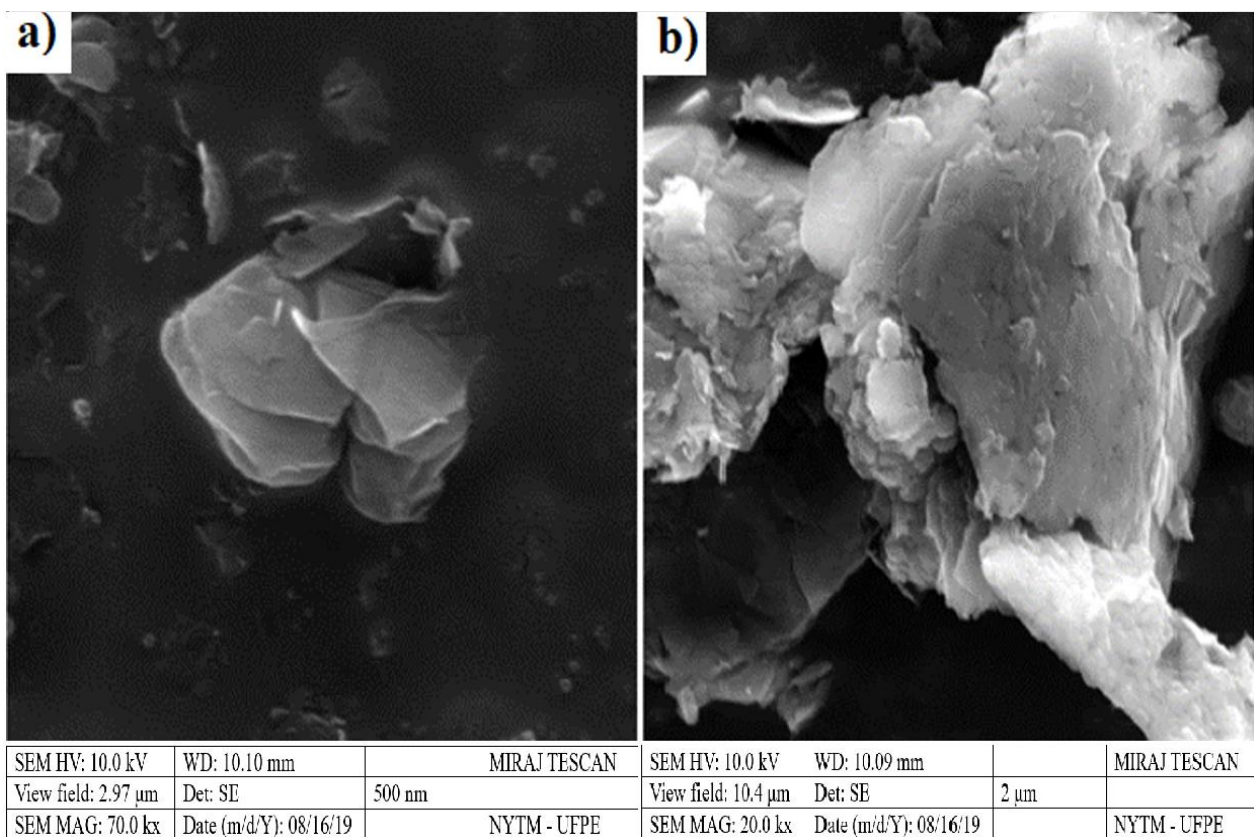


Figure 1. SEM image of a graphene nanosheet: (a) 500 nm; (b) 2 μm.

For analysis of nanoparticle stabilization in the graphene nanofluid, time-sequenced sample decantation tests were performed at 0, 4, and 24 h for the exfoliated graphite. Sodium Lauryl Ether Sulfate (Lauryl) and Sodium Polystyrene Sulfonate (PSS) were used as surfactants, which are the two most commonly reported in the literature for use in heat exchanger nanofluids. Two observations can be made: Lauryl showed greater temporal stability than PSS; and after 24 h, Lauryl presented no sedimentation or agglomeration of the nanoparticles, with visual inspection, indicating that it allows the formulation of nanofluids that have a lower tendency to precipitation in use, verifying the stability of graphene nanofluids in heat exchange processes. These analyses are consistent with the literature [41,42].

Figure 2 presents the diffractograms obtained from the commercial graphite powder and the sample obtained by the electrochemical process of exfoliation, through the technique of X-ray diffraction (XRD) performed using a model XRD-7000 (Shimadzu Cor-

poration, Kyoto, Japan) diffractometer. The deflection of the angle of the X-ray beam is presented horizontally and the intensity vertically.

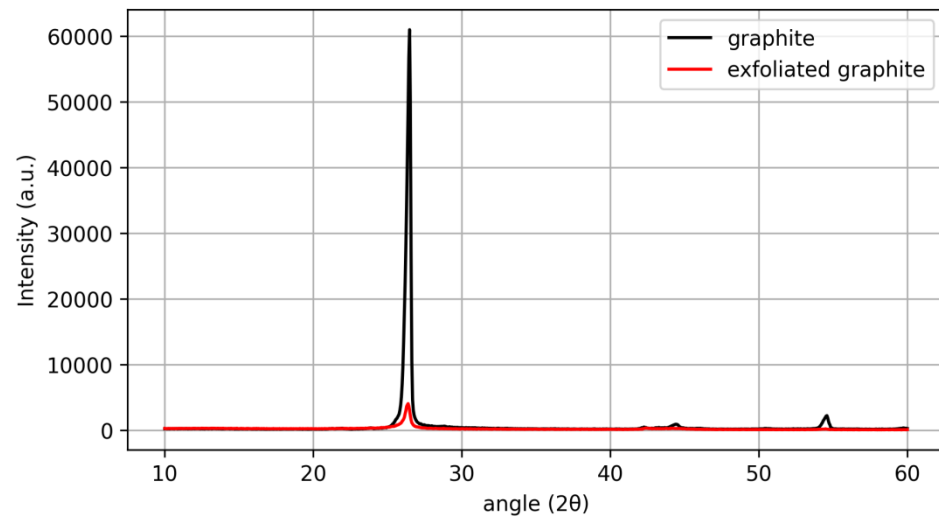


Figure 2. Diffractograms of graphite samples.

The exfoliated graphite sample shows the same diffraction peaks as the powdered graphite, but with a reduced intensity, which indicates a smaller amount of material presenting the same crystallinity as the graphite. The maximum position of the peak appears at $2\theta = 26.5$, which is attached to the exfoliated graphite $2\theta = 26.8$, clearly demonstrating that the material is considered as a line structure. This can be interpreted as a strong indication for the efficiency of the exfoliation performed. Based on properties reported by other researchers [43,44], the XRD structure corresponds to the structure of GNP.

Figure 3 shows the sedimentation process of the GNP nanofluid. Owing to the concentration of nanofluids, sedimentation is observed after 48 h of rest. However, the pumping system of the analyzed heat exchanger was able to redisperse the nanoparticles, and changes in the thermal performance of the nanofluid after the repetitions of the experiments were not observed.

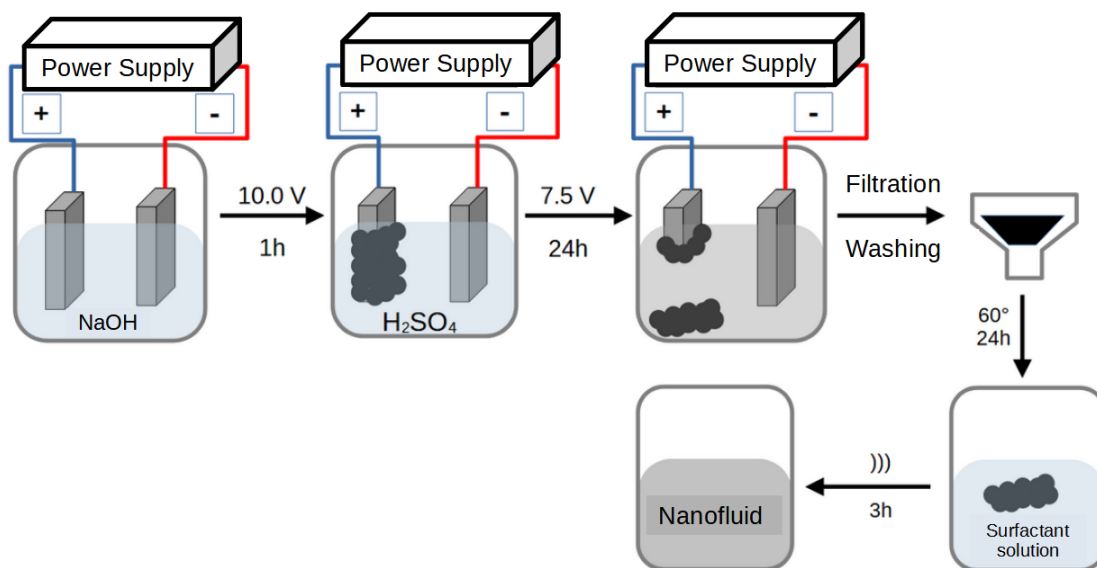


Figure 3. Sedimentation of the GNP nanofluid.

3. Experimental Setup and Procedure

For the experimental analysis, a test bench was used, as shown in Figure 4. The tests were performed with water/water and GNP/water fluids, with the nanofluid for the hot-fluid circuit and water for the cold-fluid circuit, with counterflow direction. The nanofluid concentrations were varied by weight, 0.0125%, 0.025%, and 0.050%, with operating temperature at 50 and 60 °C, flow rates of 2.5, 2.0, 1.5, 1.0, and 0.5 L/min for the hot circuit, and a constant 2.5 L/min for the cold circuit. The Reynolds numbers were between 2000 and 6000. The system used K-type thermocouple temperature measuring sensors with a resolution of 0.1 °C for the external and internal temperature reference, and an instrument error of 0.05 °C for the measurement of temperature. For the measurement of the volumetric flow of the fluids, manually adjusted turbine-type flow meters with an accuracy of $\pm 1\%$ were used. A proportional–integral–derivative (PID) controller with an electric resistance was used to heat the hot fluid, and a 7 L capacity storage tank and a centrifugal pump were used for recirculating and storing the fluid of the hot circuit, which operates within a closed loop.

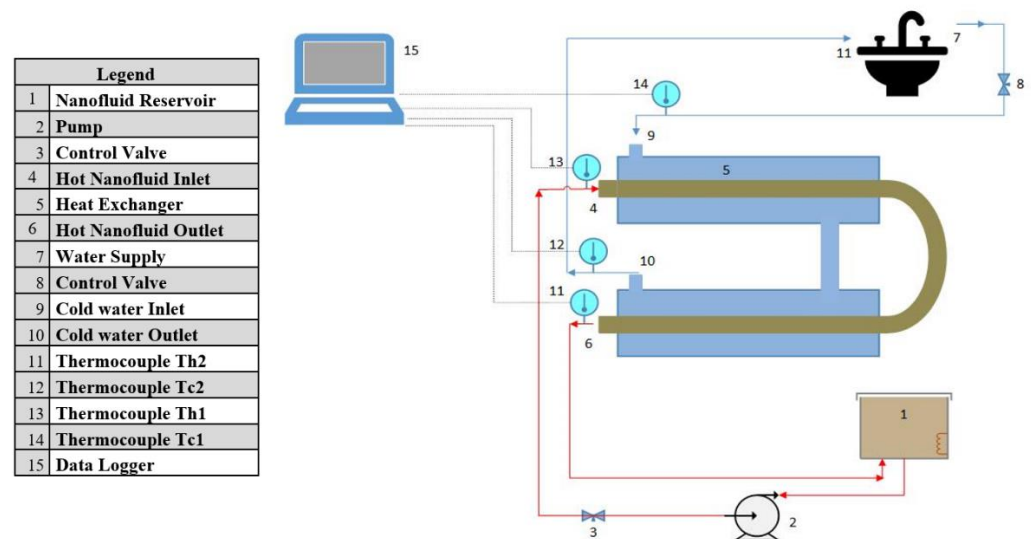


Figure 4. Schematic diagram of the DTHE experimental system.

The cold-water circuit of the test bench is connected to an external water supply from the city's supply network, making it an open circuit. This heat exchanger has thermocouples at the inlets and outlets of the hot and cold fluids, as well as thermocouples for checking the average temperatures of the circuits. Ten readings were obtained at intervals of 1 s each, for each flow rate, totaling 50 readings for each fluid, 200 in all for each temperature, through the VDAS software of the bench. All the information collected is stored for analysis and statistical treatment.

Table 1 shows the values for the statistical analysis of the uncertainties and errors of the collected data. These errors were within $\pm 1\%$, indicating that there is good agreement between the data. The results prove the reliability of the test bench for heating, transfer, and fluid flow measurements.

Table 1. Average percentage of measurement errors.

Experiments	Nanofluids	Errors (%)
1	Water	± 1.0
2	0.0125	± 1.0
3	0.025	± 1.0
4	0.050	± 1.0

3.1. Heat Exchanger DTHE

The double tube heat exchanger (DTHE), shown in Figure 5, is the simplest exchanger used in processes, consisting of two concentric tubes of different diameters, usually with two straight sections and with appropriate connections at the ends of each tube. In this design, one fluid flows through the smaller tube while the other flows through the annular space between the two tubes. The heat exchange occurs through the wall of the inner tube [45,46].

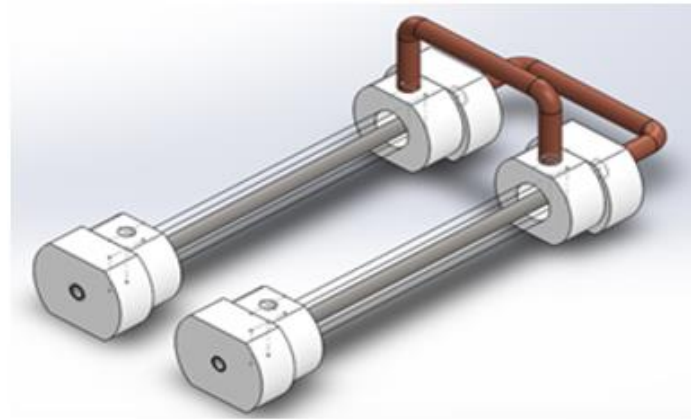


Figure 5. DTHE CAD modeling.

Table 2 shows the complete specifications of the heat exchanger used on the test bench. The main advantages of this type of exchanger are the ease of construction, assembly, area expansion (i.e., additional area can be installed in an existing unit), and maintenance, with easy access for cleaning on both sides of flow, depending on the end connections [47].

Table 2. Technical specifications of the DTHE.

Items	Specification	Items	Specification
Breadth (mm)	500	External diameter (mm)	30
Depth (mm)	260	Internal diameter (mm)	20
Height (mm)	160	Inner tube:	Material: stainless steel
Weight (kg)	3.5	External diameter (mm)	1
Shell tube (outer):	Material: transparent acrylic	Internal diameter (mm)	10
Average transfer area of heat (m ²)			0.02

3.2. Thermophysical Properties of GNP/Water Nanofluids

For the analyzed thermophysical properties of the nanofluids with graphene nanoparticles, a KD2 Prothermal needle from Decagon Devices, Inc. (Pullman, WA, USA), was used. It uses the transient hot-wire method to measure the thermal conductivity with an accuracy of $\pm 5\%$. A Haake Viscotester 6 L plus viscometer measured the viscosities of the nanofluids, and the measurement of their densities was performed by electronic weighing and by Equation (1), using a pycnometer and a precision balance. The specific heats were calculated using the method of Xuan and Roetzel [48], in which they modified the model of Pak and Cho [49] by considering the difference between the specific masses of the nanoparticles and the base fluid, thus proposing a new model shown in Equation (2).

$$\rho = \frac{M_{nf}(\text{kg})}{V_{nf}(\text{m}^3)} \quad (1)$$

$$C_{nf} = \frac{(1 - \varnothing_V)\rho_{fb}C_{p,fb} + \varnothing_V\rho_{np}C_{p,np}}{(1 - \varnothing_V)\rho_{fb} + \varnothing_V\rho_{np}} \quad (2)$$

Table 3 presents the results of the thermophysical properties of graphene nanofluids at 25 °C used in the experimental tests and CFD simulation on the DTHE.

Table 3. Thermophysical properties of graphene nanofluids.

wt (%)	k (w/mK)	ρ (Kg/m ³)	μ (Kg/ms)	Cp (J/kg.k)	T (°C)
Water	0.62	937.5	0.000891	4120.0	25
0.0125	0.57	947.1	0.000919	3842.0	
0.025	0.6	964.0	0.000948	3846.1	
0.050	0.63	971.5	0.001008	3854.5	

Thermal conductivity is an essential parameter to be studied and analyzed when considering nanofluids [50]. The literature recommends not using low concentration percentages to avoid increased viscosity and sedimentation of the nanofluid [51,52]. Although there is a slight decrease in the thermal conductivity of the nanofluid with the base element (water), the values were very similar, with maximum relative differences of 8% for the concentration of 0.0125 wt% and minimum of 3% for the concentration of 0.025 wt%; however, in the case of the concentration of 0.050 wt%, there was a slight increase of approximately 1.6%. These values found follow a similar behavior to that discussed in the work of Yarmand et al. [51], where for concentrations of 0.06 wt% and 0.02 wt%, the thermal conductivity values were 0.60 and 0.631, respectively, being within the range of experimentation due to the uncertainties in the experimental measurements. It is essential to point out that the thermal conductivity coefficient tends to increase with increasing concentration and/or temperature; however, there is no rule of proportionality or linearity since the volumetric fraction is related to the nature of the hybrid nanoparticle and the fluid base selected. The improvement in the effective thermal conductivity is linked to the high thermal conductivity of the GNPs and Pt nanoparticles. The increase in the concentration of nanoparticles tends to decrease the distance between particles (free path) due to the percolation effect. This type of behavior has been reported and discussed in the literature [10,31,34,52].

The order of the tests and the concentrations of graphene nanofluid by weight (wt%) used can be seen in Table 4.

Table 4. Tests with graphene.

Experiments	Cold	Hot	Weight Concentration (wt%)
1	Water	Water	Water
2	Water	Graphene	0.0125
3	Water	Graphene	0.0250
4	Water	Graphene	0.0500

3.3. Experimental Data Processing

All data from the experiments were collected and recorded by the Versatile Data Acquisition System (VDAS) with values of the inlet and outlet temperatures for the hot and cold circuit together with their flow rates. The initial parameters are calculated using the following equations [53]:

$$A = \pi D_i L \quad (3)$$

$$\dot{m} = \rho VA \quad (4)$$

$$V = \frac{4\dot{m}}{\rho \pi D_H^2} \quad (5)$$

The heat transfer rates and their average rate can be calculated using the following equations [54]:

$$q_w = \dot{m}_w C p_w (T_{c2} - T_{c1})_w \quad (6)$$

$$q_{nf} = \dot{m}_{nf} C p_{nf} (T_{h2} - T_{h1})_{nf} \quad (7)$$

$$Q_{ave} = \frac{q_{nf} + q_w}{2} \quad (8)$$

The convective heat transfer coefficient (Equation (10)), where phase change of a fluid occurs, can be expressed and calculated by Newton's law for cooling [55].

$$q'' = \frac{Q_{ave}}{A} \quad (9)$$

$$h = \frac{q''}{T_{wall} - T_{nf}} \quad (10)$$

The method used to choose a heat exchanger that allows for achieving a specific temperature change with known mass flow rates is the logarithmic mean temperature difference (LMTD) method [56]:

$$\Delta T_{LMTD} = \frac{\Delta T_2 - \Delta T_1}{\ln\left(\frac{\Delta T_2}{\Delta T_1}\right)} \quad (11)$$

where ΔT_1 and ΔT_2 are the temperature differences between the hot and cold fluid at both ends (inlet and outlet) of the heat exchanger.

$$\Delta T_1 = T_{H2} - T_{C1} \quad (12)$$

$$\Delta T_2 = T_{H1} - T_{C2} \quad (13)$$

Through Equations (3), (9) and (11) the overall heat transfer coefficient (U) can be calculated using the relationship reported by Bahiraei and Monavari [4]:

$$U = \frac{Q_{ave}}{\Delta T_{LMTD} A} \quad (14)$$

The Reynolds number can be calculated using Equations (15a) and (15b), which represent the calculated Reynolds number for the tube and annulus, respectively [57].

$$Re_{nf} = \frac{\rho V D_i}{\mu} = \frac{4\dot{m}}{\pi D_i \mu} \quad (15a)$$

$$Re_w = \frac{\rho V D_h}{\mu} = \frac{4\dot{m}}{\pi (D_e + D_i) \mu} \quad (15b)$$

To determine the friction factor for the nanofluids, Equation (16) was used, according to the pressure drop in the test section [58].

$$f = \frac{\Delta P}{\frac{L}{D} \frac{\rho V^2}{2}} \quad (16)$$

The Nusselt number and Prandtl number can be calculated using Equations (17) and (18), respectively [59].

$$Nu = \frac{H D_H}{k} \quad (17)$$

$$Pr = \frac{C_p \mu}{k} \quad (18)$$

To find the pressure drop (ΔP) associated with the additional height that must be increased to the fluid by the pump used, Equation (16) is applied. Once the pressure drop is known, the power required at the pump (Pumping Power— \dot{W}) to overcome the flow resistance associated with this pressure drop can be determined from Equation (19) [60].

$$\dot{W} = \frac{\dot{m} * \Delta P}{\rho} \quad (19)$$

The heat transfer effectiveness (ε) (Equation (22)) in a heat exchanger is defined through Equation (9) and the maximum possible heat transfer rate (q_{max}). The latter can be determined through Equation (21), where C_{min} is the lowest value found among the heat capacity rates (Equation (20)) [24].

$$C_w = (\dot{m}C_p)_w \quad (20a)$$

$$C_{nf} = (\dot{m}C_p)_{nf} \quad (20b)$$

$$q_{max} = C_{min}(T_{h1} - T_{c1}) \quad (21)$$

$$\varepsilon = \frac{Q_{ave}}{q_{max}} \quad (22)$$

To determine the efficiency (η) (performance index) regarding thermal exchange with the use of graphene-based nanofluids in comparison to water, Equation (23) [61].

$$\eta = \frac{Q_{ave}}{\Delta P} \quad (23)$$

4. CFD Modeling and Mesh Generation

Computational modeling of the double tube heat exchanger was performed by applying the CFD method, using SolidWorks for the physical modeling and separating the solid and fluid domains. To model the turbulent flow in the investigation and ensure the accuracy of the results, the k- ε model was implemented in the numerical procedure, including all transport equations representing the tuflow's turbulent properties for internal and bounded flows and the wall boundary condition [54]. This model was used since it is the most common model using CFD to simulate medium flow characteristics for turbulent flow conditions. The k- ε model is a two-equation model that provides a general description of turbulence using two transport equations.

Simulations were performed using the same geometry and dimensions as those for the DTHE in the experimental tests and under the same operating conditions. Figure 6 shows the heat exchanger model via CFD, with the hot-nanofluid (red) and cold-water (green) flow circuit differences. The boundary conditions used in the CFD simulation were inlet, outlet, and wall.

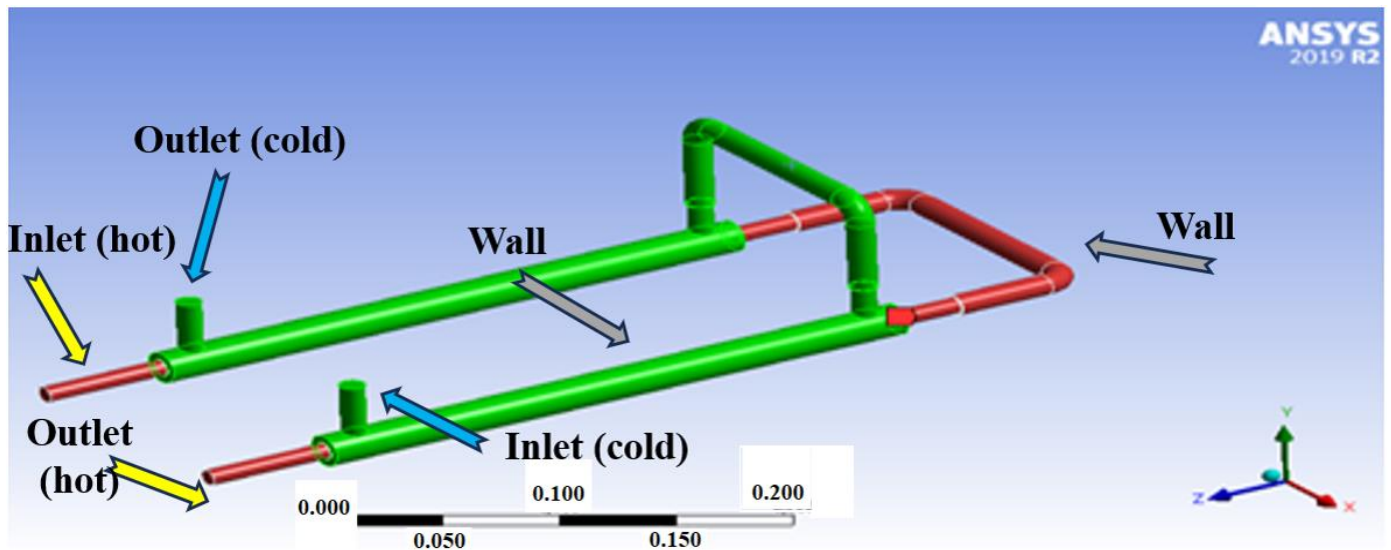


Figure 6. CFD double tube heat exchanger 3D model.

For mesh generation, ANSYS meshing was used, considering a tetrahedral mesh through the skewness quality metric, with 70,077 elements, as shown in Figure 7.

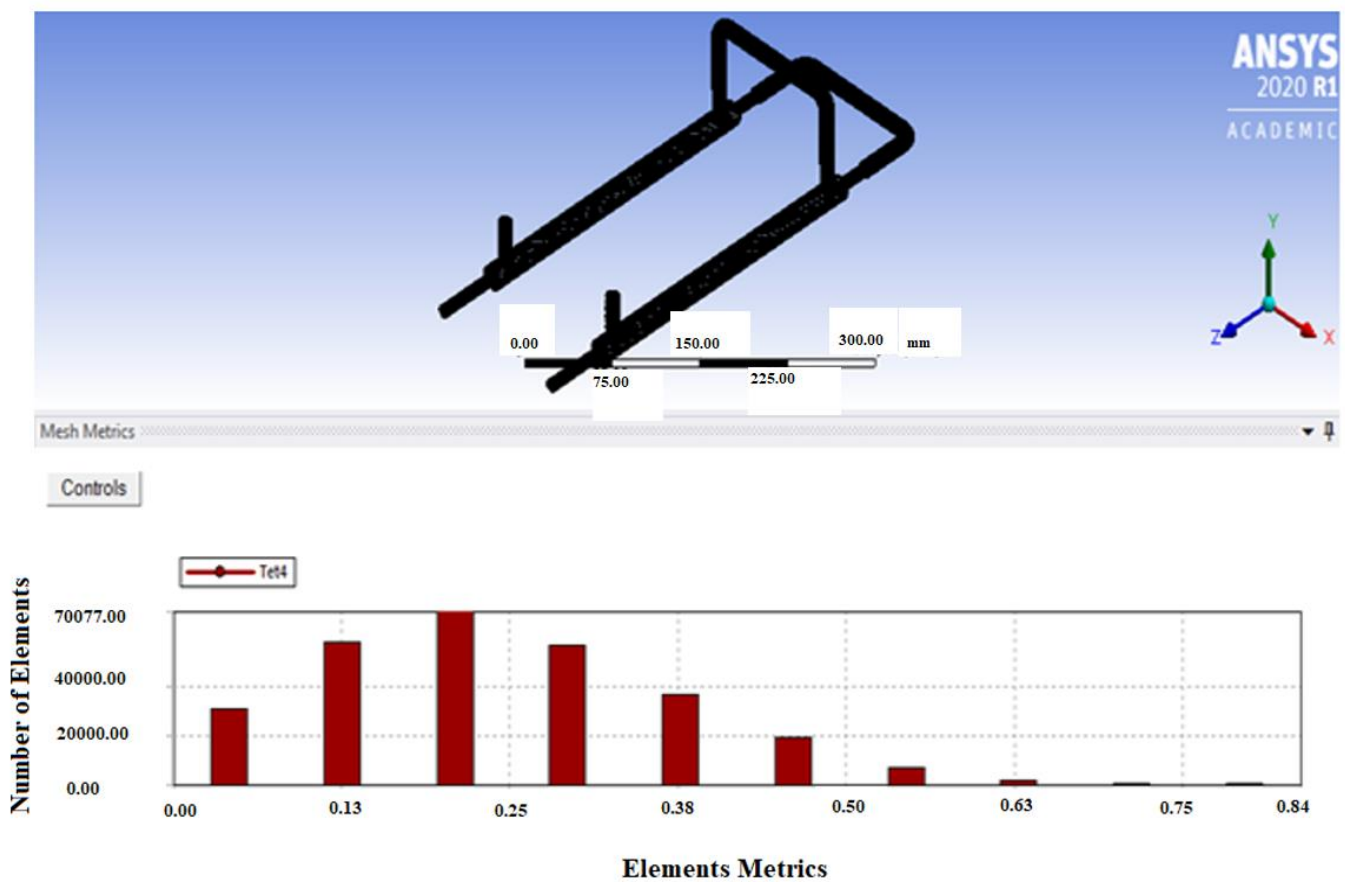


Figure 7. Mesh with element numbers.

The analysis of the mesh was based on validation with experimental results using water as the working fluid. This approach eliminated the need for further refinement of the mesh since it was already refined to an error tolerance with the experimental data. The

mesh was verified through mesh analysis, which involved checking the gain in accuracy with the increase in the number of nodes. The criterion used for this analysis was based on the accuracy of the K-type thermocouples used in the experiment, which had an accuracy of 2% of the reading value. The gain in accuracy was found to be below 1%, indicating that the mesh was sufficiently accurate for the experiment.

In different views, Figure 8 illustrates the monitoring points corresponding to the thermocouple positions equal to the real model, for validation purposes of the CFD model. The solver used was ANSYS CFX, which is based on the finite volume technique and combines an advanced solver with powerful pre- and post-processing features. The CFX solver is responsible for solving the Navier–Stokes equations and other equations inserted to establish the heat and mass transfer phenomena through the finite volume method [62]. Initially, the heat exchanger operation was simulated with water only in the two flow circuits to validate the model accuracy by comparing the numerical and experimental results.

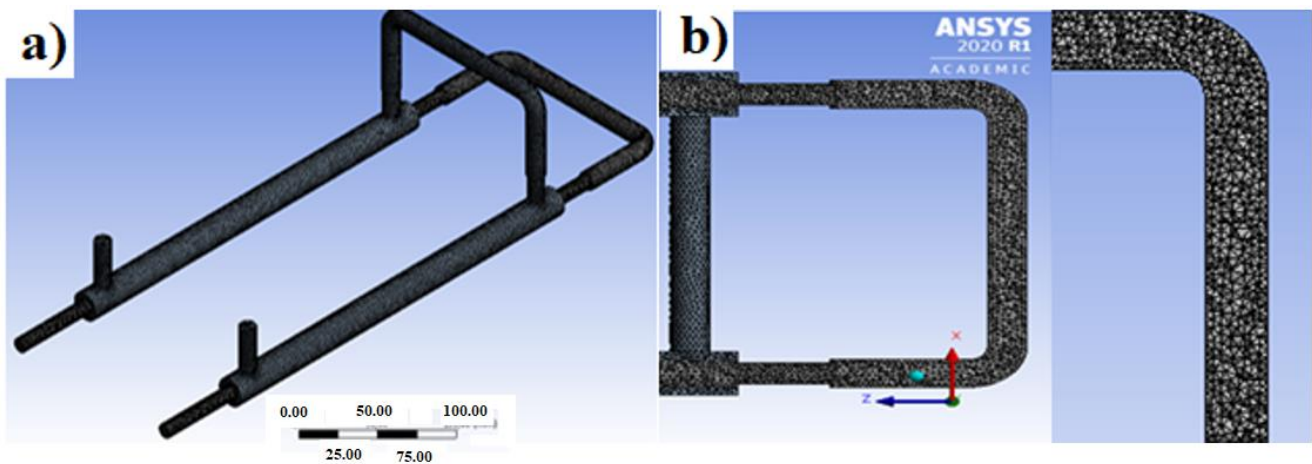


Figure 8. Computational mesh: (a) 3D model and (b) in section.

Governing Equations

To analyze the nanofluids in the heat exchangers, transport equations were used. Conservation of mass, conservation of momentum (Navier–Stokes), and conservation of energy were solved with effective properties. The fluids were considered Newtonian with permanent incompressible flow, with single-phase turbulent countercurrent motion in smooth tubes, i.e., no roughness in the flow. The relevant governing equations in their general forms are as follows [56]:

Conservation of mass:

$$\nabla \cdot (\rho \vec{v}) = 0 \quad (24)$$

Conservation of momentum:

$$\nabla \cdot (\rho \vec{v} \vec{v}) = -\nabla p + \nabla \cdot (\mu \nabla \vec{v}) \quad (25)$$

Conservation of energy:

$$\nabla \cdot (\rho \vec{v} C_p T) = \nabla \cdot (k \nabla T) \quad (26)$$

5. Results and Discussion

The exposition of the results is firstly performed through the validation of the experimental and numerical analyses in the heat exchanger using only water and comparing with other models under study, through the analyses of the Nusselt number and the fric-

tion factor. Subsequently, the analyses of the results for the heat exchanger in the energy behavior parameters are presented.

5.1. Comparison of the Results (Numerical–Experimental) Validation of Study

The nondimensional Nusselt numbers were used as validation parameters for the numerical study. Experimental data were used to compare with those predicted by standard correlations to validate the test bench and evaluate the measurement uncertainties. The empirical correlations used for determining the Nusselt numbers from the experimental data were Dittus–Boelter [63,64], Gnielinski [65], and Petukhov [66], respectively, Equations (27)–(29) (see Table 5). The Nusselt number considered was for fluids in completely developed turbulent single-phase flows in smooth tubes. The Dittus–Boelter equation is one of the most often used equations in the literature, but with implicit errors up to 25%. However, the last two equations are more complex, but with better accuracy and considerably reduced errors, around 10%. Figure 9 shows the comparison of the experimental results through the empirical correlations: Dittus–Boelter (Equation (27)), Gnielinski (Equation (28)), and Petukhov (Equation (29)), with the values numerically determined through the model developed via CFD.

Table 5. Empirical correlations used to determine the Nusselt number.

$Nu = 0.023Re^{\frac{4}{5}}Pr^n$	$Re \geq 10,000$ $0.7 < Pr < 160$ $\frac{L}{D} \geq 10$	(27)
$Nu = \frac{\frac{f}{8}(Re-1000)Pr}{1+12.7(\frac{f}{8})^{0.5}(Pr^{\frac{2}{3}}-1)}$	$2300 < Re < 5 \cdot 10^6$ $0.5 < Pr < 2000$	(28)
$Nu = \frac{\frac{f}{8}RePr}{1.07+12.7(\frac{f}{8})^{0.5}(Pr^{\frac{2}{3}}-1)}$	$10^4 < Re < 5 \cdot 10^6$ $0.5 < Pr < 2000$	(29)

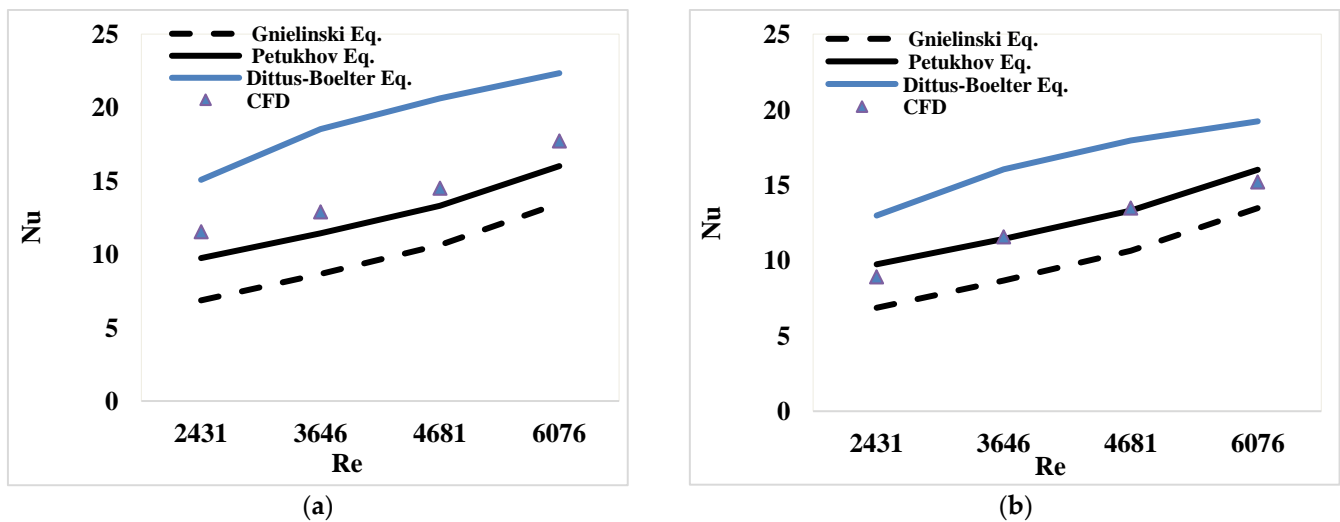


Figure 9. Comparison of the CFD numerical and experimental results through the empirical correlations: (a) fluid temperature 50 °C; (b) fluid temperature 60 °C.

Figure 9a,b present the experimental results using the empirical correlations, considering the average fluid temperatures of 50 and 60 °C, for the calculation of the Nusselt numbers (Nu) in the DTHE and through the CFD simulated with water, as a form of validation between the numerical and experimental models, respectively.

The values of the Nusselt numbers determined from the experiments showed good agreement with those calculated by the empirical correlations and the CFD model, being able to simulate the heat transfer characteristics of graphene-based nanofluids. The largest relative errors found between the correlations and the numerical model values were 31%,

36%, and 9%, and the smallest relative errors were 21%, 13%, and 1% for the Dittus–Boelter, Gnielinski, and Petukhov correlations, respectively. Besides the error propagation in the experimental values, approximately 5%, this emphasizes that even with these divergences the values obtained are within the ranges considered by the numerical and experimental uncertainties of the correlations. Therefore, it can be stated that the model developed via CFD was able to adequately represent the behavior of the convective heat transfer coefficients for the double tube heat exchanger. Furthermore, one can see that the divergence between numerical and experimental values was found with the use of the Petukhov equation, which more accurately represents the Nusselt number values, thus confirming that the model can accurately reproduce the results found in the actual operation of the double tube heat exchanger, with maximum and minimum relative error values of 9% and 1%. The results in Figure 8a,b show similar behavior to those presented in the literature [67–69].

A relative difference between the results found experimentally and those obtained numerically was observed, in some cases analyzed, due to the materials used, deviations in the thermophysical properties of the nanofluids, and even in the uncertainties of the sensors and equipment used in the measurements. One of them is the type of water used in the experiments, which was supplied by the utility in the state, and has minerals and impurities, which were not taken into consideration in the numerical simulation due to the increased complexity in the model. Another source of deviation might be the lack of a better mesh refinement that would help approximate the experimental results. Finally, the environmental conditions to which the exchangers are exposed (external natural convection), were not considered in the CFD simulation performed and might also be a source of errors.

The CFD analysis showed great potential in representing the thermohydraulic behavior of heat exchangers using graphene nanofluid for other concentrations, thereby increasing the scope of the analysis, in addition to the results found in the experimental tests.

5.2. Behavior of the Nanofluids and the Water on the DTHE

This section shows the behavior resulting from the addition of graphene nanoparticles in water to verify the thermal and hydraulic performance, and its overall behavior effect when compared to the heat exchanger reference fluid, in this case, water.

5.2.1. Nusselt Number Behaviors of the Nanofluids and the Water on the DTHE

The behavior of the Nusselt numbers for pure water and graphene nanofluids with concentrations of 0.0125, 0.025, and 0.05 wt% was analyzed based on experimental results.

Figure 10a (left side) and Figure 10b (right side) show that the addition of graphene nanofluids to the general fluid results in an energy gain for thermal performance in heat exchange in the DHTE. For instance, the Nusselt numbers with the nanofluid of 0.025 wt% concentration by weight showed a percent increase of 6.66% and 4.89% compared to water.

In contrast, for the simulated results, the highest Nusselt number was found for the 0.0125 wt% concentration (Figure 9a) compared to water, which was 3.44%. The lowest standard error found was for the experimental and CFD nanofluid concentration of 0.025 wt% and 1.36%, as shown in Figure 9a. This analysis can also be seen in the literature [57,70].

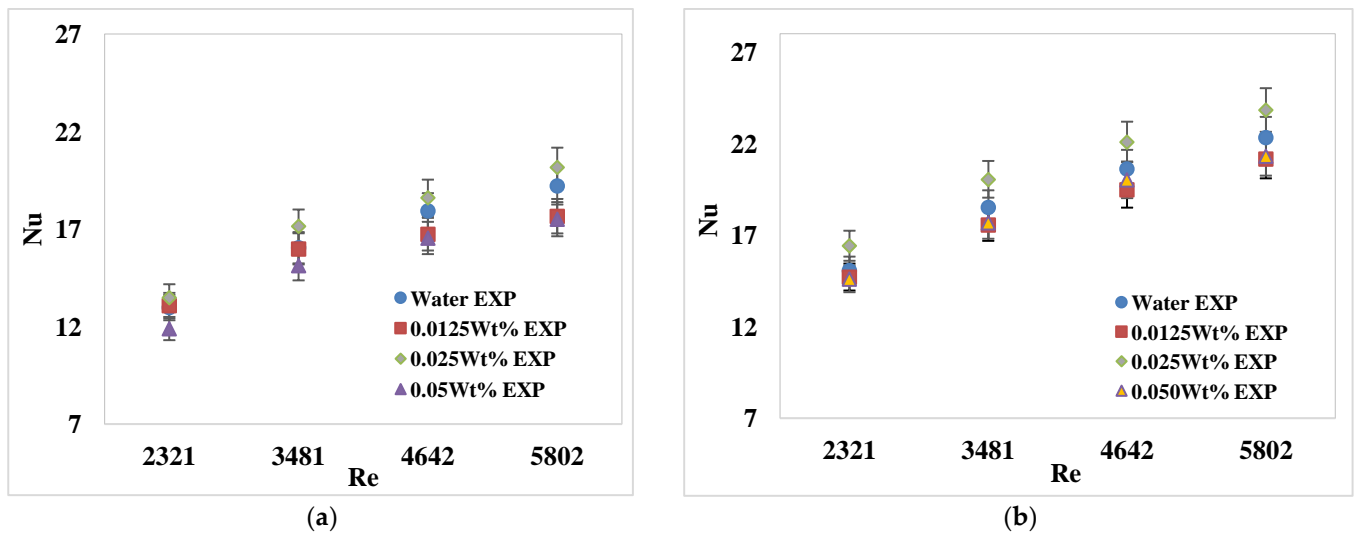


Figure 10. Behavior of Nusselt numbers as a function of Reynolds number considering water as the reference fluid, and graphene nanofluids with 0.0125, 0.025, and 0.050 wt% concentrations: (a) fluid temperature 50 °C; (b) fluid temperature 60 °C.

5.2.2. Friction Factor Behavior of the Nanofluids and the Water on the DTHE

The correlations for the friction coefficients in turbulent flows were based on experimental studies, as it is difficult to manage turbulent flow theoretically [71]. This procedure of comparing results has been used in several studies of flow and correlations, as can be seen in the literature [72,73].

An important parameter to be verified in heat exchangers is the friction factor as a function of the pressure drop along the equipment. Therefore, the following correlations were considered to evaluate this parameter: Petukhov [67], Blasius [74], Von Kármán [75], Prandtl [71], and Colebrook [76], as shown in Table 6.

Table 6. Equations used to determine the friction factor.

$f = (0.790 \ln(Re) - 1.64)^{-2}$ $2300 < Re < 5 \cdot 10^6$	(30)			Petukhov [66]
$f = 0.3164 Re^{-0.25}$ $3000 < Re < 10^5$	(31)	Blasius [74]	$\frac{1}{\sqrt{f}} = -2 \log \left(\frac{2.51}{Re \sqrt{f}} \right)$	(32) Von Kármán [75]
$\frac{1}{\sqrt{f}} = -2 \log$	(33)	Prandtl [71]	$\frac{1}{\sqrt{f}} = -2 \log \left(\frac{2.51}{Re \sqrt{f}} + \frac{\epsilon}{3.7D} \right)$	(34) Colebrook [76]

For smooth pipes with fully developed turbulent flow, the friction factor can be calculated using the explicit Petukhov equation [66] for water as a base fluid. Stainless-steel pipes were used in this work and can be considered smooth pipes with negligible roughness.

Figure 11 presents the variation in the friction factor as a function of the Reynolds number for water, considering the correlations presented.

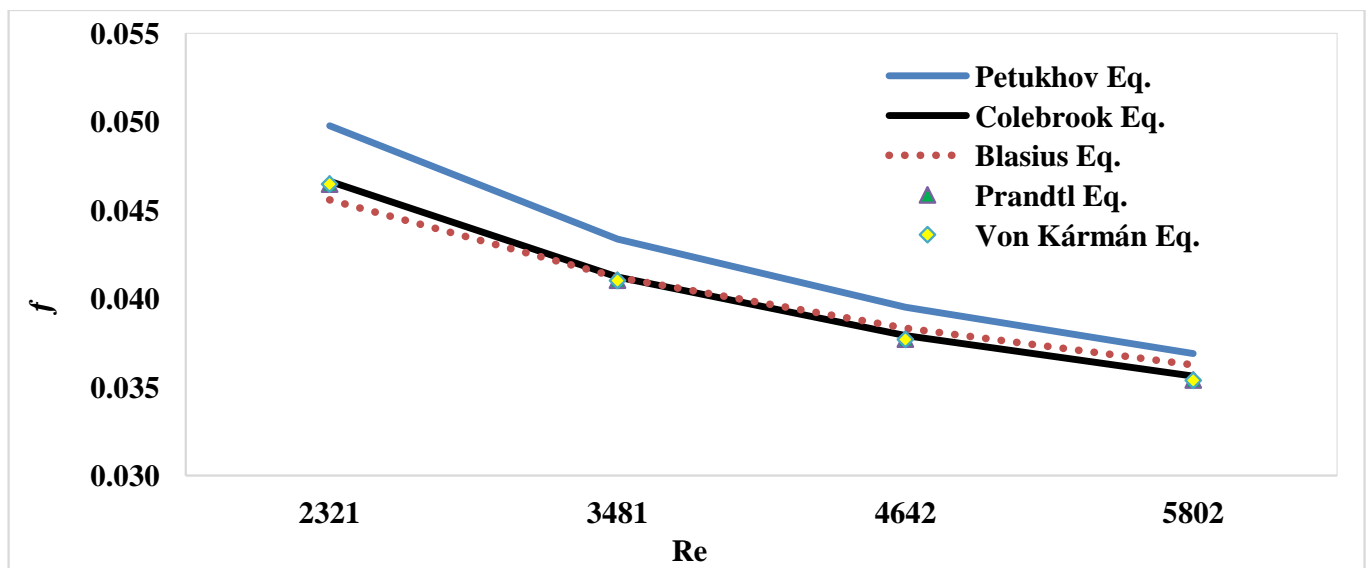


Figure 11. Behavior of the friction factor as a function of the Reynolds number through empirical correlations, considering the water as the reference fluid.

The results obtained using water as the working fluid in the heat exchangers through the empirical correlations cited in the literature [77,78] showed a coherent behavior regarding the friction factor and its relationship with the pressure drop in the system. The values found for the friction factors showed good agreement with an 8% range in maximum relative error and a minimum of 0.04% when compared to the Blasius equation. These deviations tend to be smaller for Reynolds values above 8000, where the values are almost superimposed on each other. This indicates good accuracy between the values found since it is pertinent to note that these empirical correlations present errors of uncertainty in the calculations. Furthermore, the uncertainties are within $\pm 5\%$, indicating a reliable experimental setup. Taking the values determined by the Petukhov correlation as a reference, being the one used for smooth pipes with fully developed turbulent flow, the maximum relative errors were 4.78%, 7.99%, 5.10%, and 5.13%, and the minimum ones were 0.71%, 0.04%, 1.73%, and 1.75%, among the other correlations of Colebrook, Blasius, Prandtl, and von Kármán, respectively.

Figure 12 presents the variation in the friction factor relative to the Reynolds number for water, and different concentrations of graphene nanofluids via the Petukhov equation.

There is an increase in the friction factor as the concentration of the nanofluid by weight of GNP/water increases, and at the same time, there is a decrease in this friction factor as the Reynolds number increases.

Graphene nanofluids showed slightly larger friction factors than indicated for the base fluid (water), with maximum relative errors of 1.10%, 2.19%, and 4.46% for the concentration of 0.0125, 0.025, and 0.050 wt% respectively. The friction factors of the GNP/water nanofluids in this study are similar to the results reported in several works [57,79,80] that used graphene nanofluids. Therefore, although the values of the factors are larger, the ranges for the values are insignificant and are within the error uncertainties ($\pm 5\%$), and the errors are extended by Petukhov's empirical correlation.

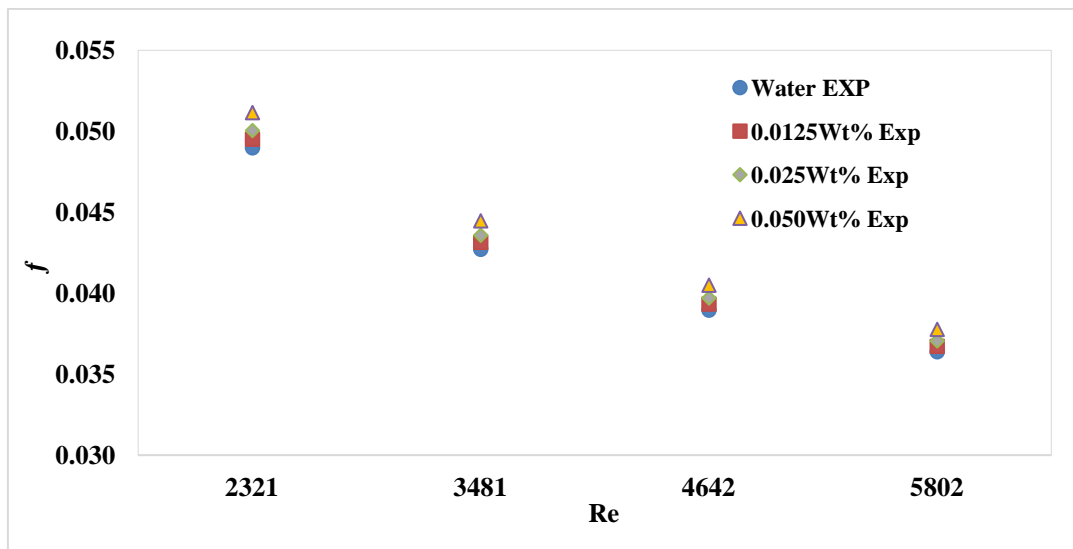


Figure 12. Behavior of the friction factor as a function of the Reynolds number through empirical correlations, considering the water as a reference fluid and the graphene nanofluids with concentrations of 0.0125, 0.025, and 0.05 wt%.

5.2.3. Pressure Drop Behavior of the Nanofluids and the Water on the DTHE

As an identifying parameter on the hydrodynamic behavior of the addition of graphene nanofluids in water, the pressure drop calculation and the energy power value for the pumping system drive along the heat exchanger were introduced.

Figure 13 shows the values of pressure drop (a—left) and power consumed by the system pump (b—right) along the heat exchanger as a function of Reynolds number, using the friction factor calculated by Petukhov's correlation. The friction factor and the load losses were calculated using Equations (16) and (30), respectively.

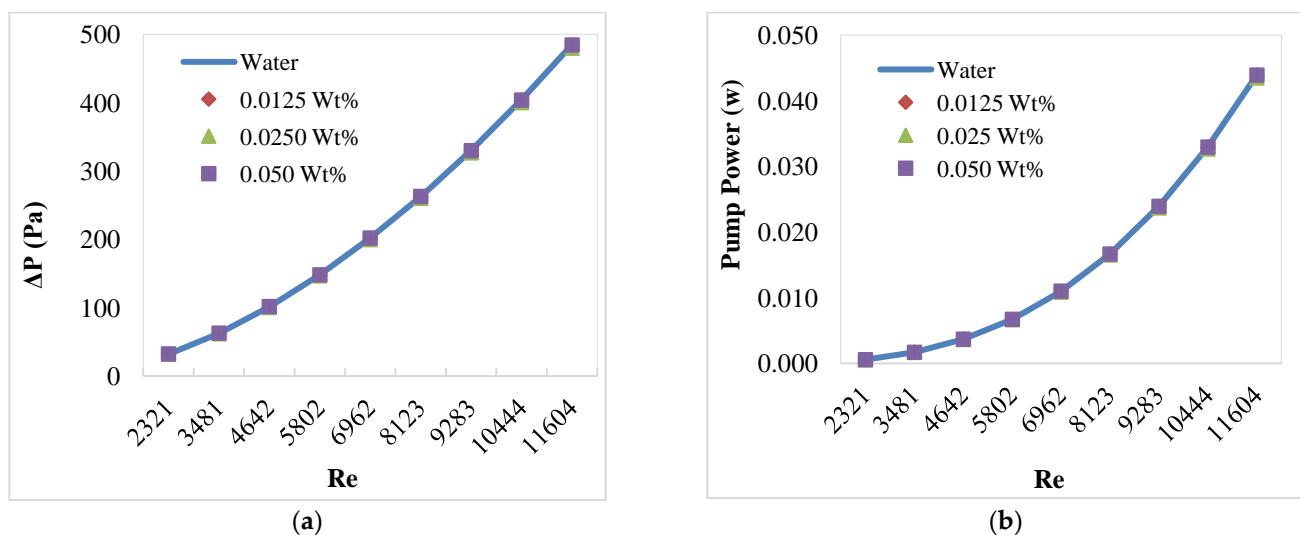


Figure 13. Behavior of the friction factor as a function of the Reynolds number through empirical correlations, considering water as the reference fluid and graphene nanofluids with concentrations of 0.0125, 0.025, and 0.05 wt%.

The experimental results, as shown in Figure 13a, indicate that the pressure drop increases along with the measured growth of the friction factor with the increment in the Reynolds number. This behavior was observed for both pure water and graphene nanofluids. The pressure drops increased as the concentration by weight of the nanofluid

increased compared to water. The relative maximum and minimum values of the pressure drop were 1.42% and 0.01% with the 0.05 %wt and the 0.0125 %wt concentration nanofluid, respectively.

The behavior of the power consumed by the heat exchanger pump (Figure 13b) was similar to that of the pressure drop (Figure 13a) since these values are directly proportional. The pumping power result was calculated using Equation (19), where the relative errors presented values of 0.16%, 1.10%, and 2.23%, for 0.0125; 0.025, and 0.050 wt%, between water and graphene nanofluids, respectively. It should be noted that the dynamic viscosity of water is lower than that of nanofluids. The highest power consumption occurs for high Reynolds numbers, with the growth rate being almost exponential. This is due to the lubricating properties of the GNP particles, thus reducing the friction between the fluid particles and the exchanger surfaces. The pumping power of the GNP/water nanofluids was close to that of water, as observed in Figure 13a,b.

The experimental results show that the pressure drop and friction factor depend on the concentration by weight of the GNP/Water and the Reynolds number, with a higher pressure drop as the concentration of the nanoparticles in the nanofluids increases. Therefore, the energy consumption required in pumping nanofluids is equal or in some cases lower when compared to water.

5.3. Parametric Analysis of Energy Behavior

A parametric analysis was performed via CFD considering the influence of the addition of the graphene nanofluids in water on the temperature profile, the overall heat transfer coefficient, and the effectiveness and efficiency of the heat exchanger used.

5.3.1. Temperature Behavior in the DTHE via CFD Simulation

The temperature profile along the DTHE heat exchanger is shown in Figure 14. At the nanofluid inlet and water outlet circuits (black circle), the convective heat transfer process was relatively low along the whole first tube. However, when the nanofluid flows through the end of the DHTE equipment (second tube of the circuit), at the nanofluid outlet and water inlet circuits (gray circle), an increase in the heat exchange was observed. The introduction of nanofluids improves heat exchange between cold (pure water) and hot (nanofluid) fluids, with a gain in average temperature of 18% using 0.050, 0.025, and 0.0125 wt% concentrations. A sensibility analysis was conducted to verify the CFD performance of the nanofluid in the heat exchanger, considering the heat exchanger's overall heat transfer coefficient, heat transfer effectiveness, and performance index, as seen in the literature [61,81].

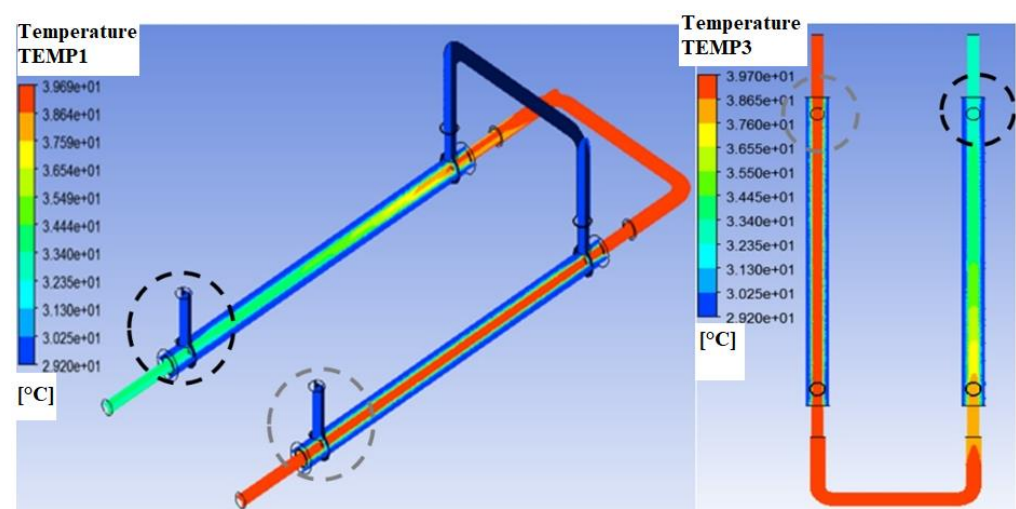


Figure 14. Temperature profile behavior of hot and cold fluids in a double tube heat exchanger.

5.3.2. Behavior of the Overall Heat Transfer Coefficient

The results of the overall heat transfer coefficient for DHTE via CFD as a function of the Reynolds number are presented in Figure 15, varying the concentrations of the graphene-based nanofluids for temperature of 50 °C in Figure 15a and 60 °C in Figure 15b, calculated using Equation (14). The results obtained with the water-based fluid showed the best performance for the overall heat transfer coefficient (U) when compared to the fluids with the introduction of the graphene nanofluids. The maximum relative difference was presented by the nanofluid at 0.0125 wt% with temperatures of 50 and 60 °C, maintaining the trend, with $U = 19\%$, and the relative difference was smaller with the fluid at 0.050 wt%, with $U = 2\%$, approximately, for both temperatures of 50 and 60 °C. However, when exclusively evaluating the fluid with nanofluid, the greater the graphene concentration in the fluid, the greater the overall heat transfer coefficient, and the greater the Reynolds number, the greater the overall heat transfer coefficient. The trend of the values obtained with the nanofluids was consistent with the results found in the literature [67,70,81], where it is verified that the higher the nanoparticle concentration in the fluid and the larger the Reynolds number (Re), the overall heat transfer coefficient tends to be higher, which is also compatible with the results shown in Bahiraei et al. [82].

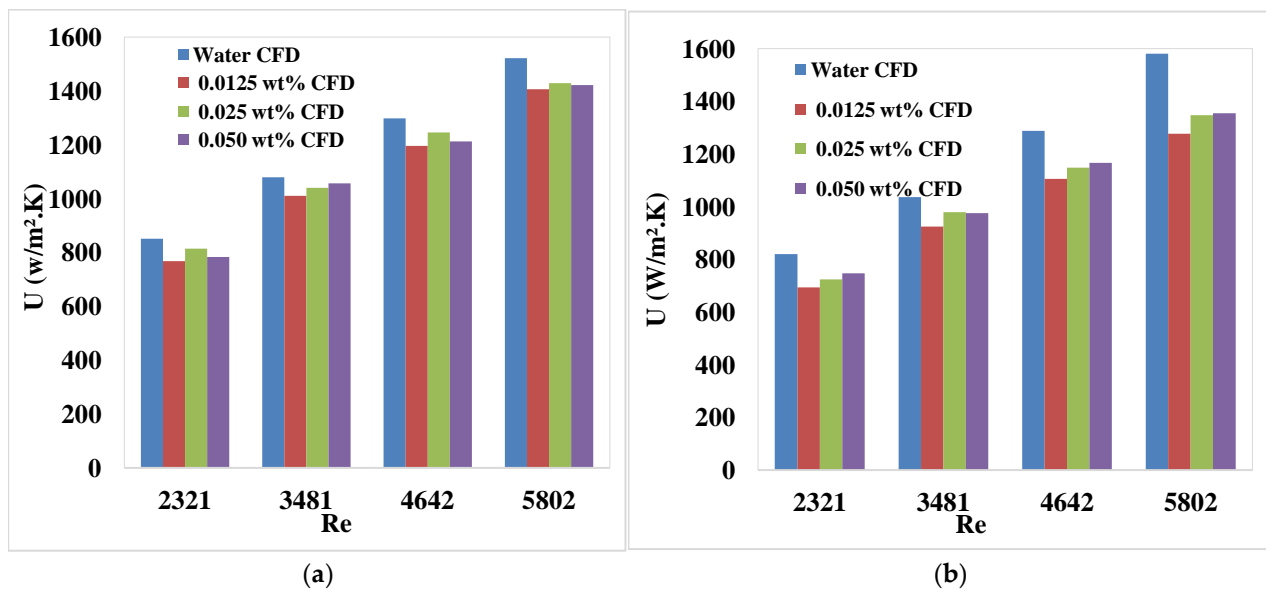


Figure 15. Behavior of the overall heat transfer coefficient for the double tube heat exchanger. (a) fluid temperature 50 °C; (b) fluid temperature 60 °C.

5.3.3. Heat Transfer Effectiveness Behavior

The thermal performance of a working fluid is evaluated by its heat transfer effectiveness in the system of a heat exchanger, as demonstrated in Figure 16. The evaluation was made through Equations (21) and (22), which presented the results in CFD versus Re , for 50 °C in Figure 16a and 60 °C in Figure 16b for the DTHE. It can be visualized that the introduction of graphene nanofluids to the system provided an improvement in the effectiveness of the heat exchanger, specifically with a higher concentration of nanoparticles, i.e., 0.050 wt%, with a percentage gain of 3%, and lower for the concentration of 0.0125 wt%, with 0.5%, compared to water. This was evident for 50 °C. This gain was significant for Reynolds number ($Re > 4000$). With increasing temperature, 60 °C, this effect changes toward having better effectiveness with the base fluid, water, and subsequently with the nanofluids, being better for the 0.050 wt% concentration and lower for 0.0125 wt%. Despite this improvement, the differences between the effectiveness values with water and the nanofluids were remarkably similar. This behavior had the same trend as the results shown in the literature [59,79,83].

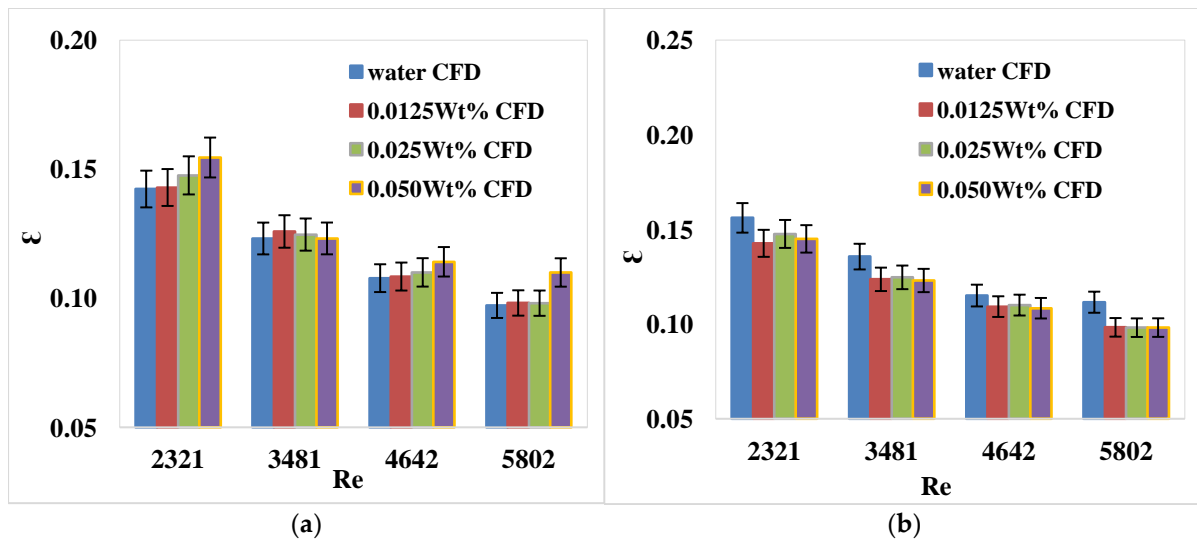


Figure 16. Behavior of the overall heat transfer coefficient of the double tube heat exchanger: (a) fluid temperature 50 °C; (b) fluid temperature 60 °C.

5.3.4. Performance Index of the Heat Exchangers

The performance index for the use of nanofluids in the double tube heat exchanger was evaluated using Equation (23). This parameter checks the behavior of the energy gain in the average heat exchange rate relative to the increase in the pressure drop in the system. Figure 17 shows the behavior of the performance index with the variation in the Reynolds number for the two analysis temperatures, 50 and 60 °C.

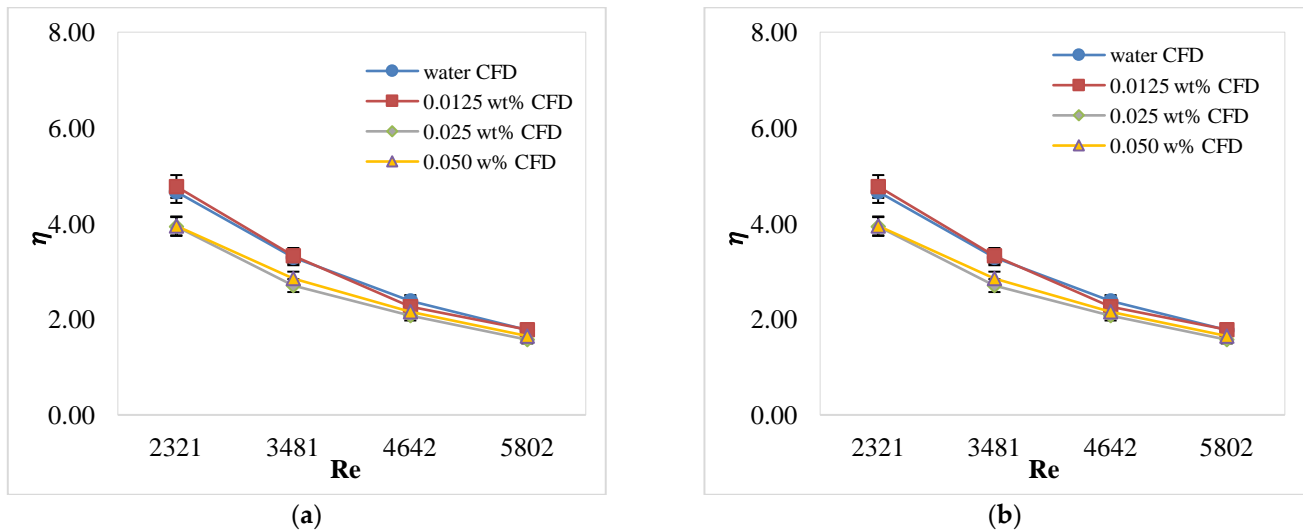


Figure 17. Performance index behavior of nanofluid in the double tube heat exchanger: (a) fluid temperature 50 °C; (b) fluid temperature 60 °C.

The results showed that with increasing temperature (50 to 60 °C) the performance index was higher. In terms of nanofluid concentrations, the lowest values provided a slightly better performance index compared to water, in the case of 0.0125 wt% concentration, with values from 5 to 2 at 50 °C and from 8 to 4 at 60 °C. It should be noted that the highest values of the performance index were found for lower Reynolds numbers. This is due to the increase in the pressure drop with the increase in the Reynolds number, which is related to the increase in the flow rate. However, for the 0.025 and 0.050 wt% concentrations, the values were lower than the performance indices obtained for water, due to the higher rate

of pressure drop growth compared to the heat exchange rate achieved by the introduction of the nanofluids. These results were consistent with the values experimentally analyzed, with the same trend regarding the concentrations. However, it can be emphasized that the size and area of the heat exchanger may have influenced the higher pressure drop, since the flow section is small and with the addition of nanofluids, the friction and the pressure to sustain the fluid flow is higher, causing this decrease in the performance index. This verifies the hypothesis that the higher the concentration of nanofluids, the higher the pressure drop, and therefore, the lower the performance index, which was also corroborated by the study presented by Bahiraei et al. [82].

6. Conclusions

From the study on the application process of graphene-based nanofluid in the double-tube heat exchanger, it was possible to verify that the evaluated parameters influence the final characteristics of the heat exchanger effectiveness. The computational model developed was able to simulate the energy behavior of the double tube heat exchanger through the CFD method. Based on the results obtained, there are some conclusions:

- The values of the Nusselt numbers determined from the experimental results showed good agreement with those calculated by the empirical correlations and the CFD model, being able to simulate the heat transfer characteristics of graphene-based nanofluids.
- The smallest divergence between numerical and experimental values was found by using the Petukhov equation, which more accurately represents the Nusselt number values, thus confirming that the model can accurately reproduce the results found in the actual operation of the double tube heat exchanger, with maximum and minimum relative error values of 9% and 1%.
- A relative difference between the results found experimentally and those obtained numerically was observed, in some cases analyzed, due to the materials used, deviations in the thermophysical properties of the nanofluids, and even in the uncertainties of the sensors and equipment used in the measurements.
- Regarding the thermal performance of the heat exchange in the DHTE when graphene nanofluids were added to the general fluid, the Nusselt numbers with the nanofluid of 0.025 wt% concentration showed a percent increase of 6.66% and 4.89% in comparison to water. In contrast, for the simulated results, the lowest Nusselt number was found for the 0.0125 wt% concentration compared to water;
- The values found for the friction factors showed good agreement with a range of maximum relative error of 8% and a minimum of 0.04% when compared to the Blasius equation. This indicates good accuracy between the values found since it is pertinent to note that these empirical correlations present errors of uncertainty in the calculations. There is an increase in the friction factor value as the concentration of the nanofluid by weight of GNP/water increases, and at the same time there is a decrease in this friction factor as the Reynolds number increases.
- Graphene nanofluids showed slightly larger friction factors than indicated for the base fluid (water), with maximum relative errors differences of 1.10%, 2.19%, and 4.46% for the 0.0125, 0.025, and 0.050 wt% concentrations, respectively. Therefore, even though the values of the factors are larger, the ranges of the values are insignificant and are within the error uncertainties ($\pm 5\%$), and the errors are extended by Petukhov's empirical correlation.
- The pressure drops increase together with the measured growth of the friction factor, with the increment in the Reynolds number. The behavior was similar for pure water, and with the graphene nanofluids. Hence, the pressure drop increased by increasing concentration by weight of the nanofluid compared to water. The relative maximum and minimum values of the pressure drop were 1.42% and 0.01% with the 0.05 wt% concentration nanofluid and the 0.0125 wt% nanofluid, respectively.

- The behavior of the power consumed by the heat exchanger pump was like that of the pressure drop since these values are directly proportional. The relative differences of the pumping power result were 0.16%; 1.10%, and 2.23%, of 0.0125 wt%; 0.025 wt%, and 0.050 wt%, between water and graphene nanofluids, respectively. It was observed that the highest power consumption occurs for high Reynolds numbers, with the growth rate being almost exponential;
- The experimental results show that the pressure drop and friction factor depend on the concentration by weight of the GNP/water and the Reynolds number, with a higher pressure drop as the concentration of the nanoparticles in the nanofluids increases. Therefore, the energy consumption required in pumping nanofluids is equal to or in some cases lower when compared to water.
- The introduction of the nanofluid in the heat exchanger improves a gain in temperature of 8 °C, i.e., approximately 28% compared to the 0.025 wt% GNP nanofluid for the base fluid, (water).
- It was verified that the results obtained with the water-based fluid showed the best performance for the overall heat transfer coefficient (U) when compared to the fluids with the introduction of the graphene nanofluids. The maximum relative difference was presented by the 0.0125 wt% nanofluid at 50 and 60 °C, maintaining the trend, with $U = 19\%$, and the relative difference was smaller with the 0.050 wt% fluid, which gave $U = 2\%$, approximately, for both 50 and 60 °C.
- The introduction of graphene nanofluids to the system provided an improvement in the effectiveness of the heat exchanger, specifically with a higher concentration of nanoparticles, i.e., 0.050 wt% with a percentage gain of 3%, being lower for the concentration of 0.0125 wt% with a value of 0.5%, compared to water. Despite this improvement, the differences between the effectiveness values with water and the nanofluids were remarkably similar.
- The results showed that with increasing temperature (50 to 60 °C), the performance index was higher. Regarding the nanofluid concentrations, the lowest values provided a slightly better performance index compared to water, in the case of 0.0125 wt% concentration, with values from 5 to 2 at 50 °C and from 8 to 4 at 60 °C. It should be noted that the highest values of the performance index were found for lower Reynolds numbers. However, for the 0.025 and 0.050 wt% concentrations, the values were lower than the performance indices obtained for water, due to the higher rate of pressure drop growth compared to the heat exchange rate achieved by the introduction of the nanofluids.
- These results were consistent with the values experimentally analyzed, with the same trend regarding the concentrations. However, it can be emphasized that the size and area of the heat exchanger may have influenced the higher pressure drop, since the flow section is small and with the addition of nanofluids, the friction and the pressure to sustain the flow of the fluid were higher, causing this decrease in the performance index.

Author Contributions: Conceptualization, C.C.X.S.L., F.D.d.M., A.A.V.O. and J.A.P.d.C.; methodology, C.C.X.S.L., F.D.d.M., A.A.V.O. and J.A.P.d.C.; software, C.C.X.S.L. and J.A.P.d.C.; validation, C.C.X.S.L., J.V.P.A., J.M.G.A.F., C.C.A.A. and J.A.P.d.C.; formal analysis, C.C.X.S.L., A.A.V.O. and J.A.P.d.C.; investigation, C.C.X.S.L., A.A.V.O. and J.A.P.d.C.; resources, F.D.d.M., A.A.V.O. and J.A.P.d.C.; data curation, G.N.P.L. and P.S.A.M.; writing—initial draft, C.C.X.S.L., F.D.d.M., A.A.V.O. and J.A.P.d.C.; writing—review and editing, F.D.d.M., A.A.V.O., G.N.P.L., P.S.A.M. and J.A.P.d.C.; visualization, A.A.V.O. and J.A.P.d.C.; supervision: F.D.d.M., A.A.V.O. and J.A.P.d.C.; project administration, F.D.d.M., A.A.V.O. and J.A.P.d.C. All authors have read and agreed to the published version of the manuscript.

Funding: This research received no external funding; only a scholarship and productivity grant, grant no. 3303417/2022-6.

Data Availability Statement: No new data were created.

Acknowledgments: The first author thanks the Federal University of Pernambuco, Federal University of Rio Grande do Norte, Federal Institute of Pernambuco, and the CAPES for a master's degree scholarship. The second author also thanks CNPq for scholarship and productivity grant no. 3303417/2022-6.

Conflicts of Interest: The authors declare no conflict of interest.

Nomenclature

A	Area	m^2	Subscripts	
C	Heat capacity	W/k	ave	Average value
c_p	Specific heat	$J/kg\ k$	bf	Base fluid
D_H	Hydraulic diameter	m	c_1	Cold-fluid inlet
f	Friction factor fanning	-	c_2	Cold-fluid outlet
h	Convective heat transfer coefficient	$W/m\ k$	e	External
L	Tube length	m	H_1	Hot-fluid inlet
\dot{m}	Mass	kg/s	H_2	Hot-fluid outlet
Nu	Nusselt number	-	i	Internal
Re	Reynolds number	-	p	Particle
\dot{v}	Average speed	m/s	max	Maximum value
\dot{W}	Pumping power	W	nf	Nanofluid
U	Overall heat transfer coefficient	$W/m^2.k$	np	Nanoparticles
T	Temperature	$^{\circ}C$	w	Water
			$wall$	Wall tube
Greek Letters			Acronyms	
ε	Effectiveness	-	$DTHE$	Double tube heat exchanger
η	Efficiency	-	GE	Grapheme
k	Thermal conductivity	$W/m\ k$	OG	Graphene oxide
μ	Dynamic viscosity	$kg/m\ s$	GNP	Graphene nanoparticles
ρ	Density	kg/m^3	NFs	Nanofluid
ΔT_{LTMD}	Temperature difference, average logarithmic	$^{\circ}C$		
ΔP	Drop loss	Pa		
ϕ	Equivalence ratio	-		

References

- Bahiraie, M.; Rahmani, R.; Yaghoobi, A.; Khodabandeh, E.; Mashayekhi, R.; Amani, M. Recent research contributions concerning use of nanofluids in heat exchangers: A critical review. *Appl. Therm. Eng.* **2018**, *133*, 137–159. [\[CrossRef\]](#)
- Esfahani, M.R.; Languri, E.M. Exergy analysis of a shell-and-tube heat exchanger using graphene oxide nanofluids. *Exp. Therm. Fluid Sci.* **2017**, *83*, 100–106. [\[CrossRef\]](#)
- Kumar, V.; Tiwari, A.K.; Ghosh, S.K. Application of nanofluids in plate heat exchanger: A review. *Energy Convers. Manag.* **2015**, *105*, 1017–1036. [\[CrossRef\]](#)
- Bahiraie, M.; Monavari, A. Thermohydraulic characteristics of a micro plate heat exchanger operated with nanofluid considering different nanoparticle shapes. *Appl. Therm. Eng.* **2020**, *179*, 115621. [\[CrossRef\]](#)
- Saldanha, W.H.; Arrieta, F.R.P.; Ekel, P.I.; Machado-Coelho, T.M.; Soares, G.L. Multi-criteria decision-making under uncertainty conditions of a shell-and-tube heat exchanger. *Int. J. Heat Mass Transf.* **2020**, *155*, 119716. [\[CrossRef\]](#)
- Maghrabie, H.M.; Attalla, M.; Mohsen, A.A. Performance assessment of a shell and helically coiled tube heat exchanger with variable orientations utilizing different nanofluids. *Appl. Therm. Eng.* **2021**, *182*, 116013. [\[CrossRef\]](#)
- Wen, T.; Lu, L.; Zhang, S.; Zhong, H. Experimental study and CFD modelling on the thermal and flow behavior of EG/water ZnO nanofluid in multiport mini channels. *Appl. Therm. Eng.* **2021**, *182*, 116089. [\[CrossRef\]](#)
- Ravi Kumar, N.T.; Bhramara, P.; Kirubeil, A.; Syam Sundar, L.; Singh, M.K.; Sousa, A.C.M. Effect of twisted tape inserts on heat transfer, friction factor of Fe₃O₄ nanofluids flow in a double pipe U-bend heat exchanger. *Int. Commun. Heat Mass Transf.* **2018**, *95*, 53–62. [\[CrossRef\]](#)
- Teng, T.P.; Cheng, C.M.; Yu, S.P. Evaluation of heat-exchange performance of carbon-based nanofluids for air-cooled exchangers with different cross-section shapes. *Appl. Therm. Eng.* **2020**, *179*, 115725. [\[CrossRef\]](#)
- Balaji, T.; Mohan Lal, D.; Selvam, C. A Critical Review on the Thermal Transport Characteristics of Graphene-Based Nanofluids. *Energies* **2023**, *16*, 2663. [\[CrossRef\]](#)
- Chakraborty, S.; Panigrahi, P.K. Stability of nanofluid: A review. *Appl. Therm. Eng.* **2020**, *174*, 115259. [\[CrossRef\]](#)

12. Tiwari, A.K.; Chatterjee, K.; Deolia, V.K. Application of Copper Oxide Nanofluid and Phase Change Material on the Performance of Hybrid Photovoltaic–Thermal (PVT) System. *Processes* **2023**, *11*, 1602. [[CrossRef](#)]
13. Pinto, R.V.; Fiorelli, F.A.S. Review of the mechanisms responsible for heat transfer enhancement using nanofluids. *Appl. Therm. Eng.* **2016**, *108*, 720–739. [[CrossRef](#)]
14. Bahiraei, M.; Mazaheri, N.; Hanooni, M. Performance enhancement of a triple-tube heat exchanger through heat transfer intensification using novel crimped-spiral ribs and nanofluid: A two-phase analysis. *Chem. Eng. Process. Process Intensif.* **2021**, *160*, 108289. [[CrossRef](#)]
15. Hajatzadeh Pordanjani, A.; Aghakhani, S.; Afrand, M.; Mahmoudi, B.; Mahian, O.; Wongwises, S. An updated review on application of nanofluids in heat exchangers for saving energy. *Energy Convers. Manag.* **2019**, *198*, 111886. [[CrossRef](#)]
16. Anitha, S.; Thomas, T.; Parthiban, V.; Pichumani, M. What dominates heat transfer performance of hybrid nanofluid in single pass shell and tube heat exchanger? *Adv. Powder Technol.* **2019**, *30*, 3107–3117. [[CrossRef](#)]
17. Gholizadeh, A.; Pourfallah, M.; Gholinia, M.; Armin, M.; Languri, E. The role of nanofluids and fins in a heat exchanger on waste energy recovery from a diesel engine: An experimental and numerical study. *Energy Rep.* **2022**, *8*, 13353–13368. [[CrossRef](#)]
18. Kasaeian, A.; Azarian, R.D.; Mahian, O.; Kolsi, L.; Chamkha, A.J.; Wongwises, S.; Pop, I. Nanofluid flow and heat transfer in porous media: A review of the latest developments. *Int. J. Heat Mass Transf.* **2017**, *107*, 778–791. [[CrossRef](#)]
19. Elbadawy, I.; Alhajri, A.; Doust, M.; Almulla, Y.; Fayed, M.; Dinc, A.; Abouelela, M.; Mahariq, I.; Al-Kouz, W. Reliability of Different Nanofluids and Different Micro-Channel Configurations on the Heat Transfer Augmentation. *Processes* **2023**, *11*, 652. [[CrossRef](#)]
20. Akyürek, E.F.; Geliş, K.; Şahin, B.; Manay, E. Experimental analysis for heat transfer of nanofluid with wire coil turbulators in a concentric tube heat exchanger. *Results Phys.* **2018**, *9*, 376–389. [[CrossRef](#)]
21. Ebrahimi-Moghadam, A.; Kowsari, S.; Farhadi, F.; Deymi-Dashtebayaz, M. Thermohydraulic sensitivity analysis and multi-objective optimization of Fe₃O₄/H₂O nanofluid flow inside U-bend heat exchangers with longitudinal strip inserts. *Appl. Therm. Eng.* **2020**, *164*, 114518. [[CrossRef](#)]
22. Khosravi, A.; Campos, H.; Malekan, M.; Nunes, R.O.; Assad, M.E.H.; Machado, L.; Pabon, J.J.G. Performance improvement of a double pipe heat exchanger proposed in a small-scale CAES system: An innovative design. *Appl. Therm. Eng.* **2019**, *162*, 114315. [[CrossRef](#)]
23. Raei, B.; Peyghambarzadeh, S.M.; Salehi Asl, R. Experimental investigation on heat transfer and flow resistance of drag-reducing alumina nanofluid in a fin-and-tube heat exchanger. *Appl. Therm. Eng.* **2018**, *144*, 926–936. [[CrossRef](#)]
24. Bashvani, I.; Eshfahani, J.A. ϵ -NTU analysis of turbulent flow in a corrugated double pipe heat exchanger: A numerical investigation. *Appl. Therm. Eng.* **2019**, *159*, 113886. [[CrossRef](#)]
25. Wijayanta, A.T.; Yaningsih, I.; Aziz, M.; Miyazaki, T.; Koyama, S. Double-sided delta-wing tape inserts to enhance convective heat transfer and fluid flow characteristics of a double-pipe heat exchanger. *Appl. Therm. Eng.* **2018**, *145*, 27–37. [[CrossRef](#)]
26. Bahmani, M.H.; Sheikhzadeh, G.; Zarringhalam, M.; Akbari, O.A.; Alrashed, A.A.A.A.; Shabani, G.A.S.; Goodarzi, M. Investigation of turbulent heat transfer and nanofluid flow in a double pipe heat exchanger. *Adv. Powder Technol.* **2018**, *29*, 273–282. [[CrossRef](#)]
27. Heeraman, J.; Kumar, R.; Chaurasiya, P.K.; Gupta, N.K.; Dobrotă, D. Develop a New Correlation between Thermal Radiation and Heat Source in Dual-Tube Heat Exchanger with a Twist Ratio Insert and Dimple Configurations: An Experimental Study. *Processes* **2023**, *11*, 860. [[CrossRef](#)]
28. Wu, Z.; Wang, L.; Sundén, B. Pressure drop and convective heat transfer of water and nanofluids in a double-pipe helical heat exchanger. *Appl. Therm. Eng.* **2013**, *60*, 266–274. [[CrossRef](#)]
29. Nagaraju, D.; Mohammad, A.R.; Santhosi, B.V.S.R.N.; Kolla, N.K.; Tota, R.K. Experimental and numerical analysis of convective heat transfer and entropy generation of graphene/water nanofluid in AEAOT heat exchanger. *J. Taiwan Inst. Chem. Eng.* **2023**, *150*, 105022. [[CrossRef](#)]
30. Jamshidmofid, M.; Abbassi, A.; Bahiraei, M. Efficacy of a novel graphene quantum dots nanofluid in a microchannel heat exchanger. *Appl. Therm. Eng.* **2021**, *189*, 116673. [[CrossRef](#)]
31. Arshad, A.; Jabbar, M.; Yan, Y.; Reay, D. A review on graphene based nanofluids: Preparation, characterization and applications. *J. Mol. Liq.* **2019**, *279*, 444–484. [[CrossRef](#)]
32. Hummers, W.S.; Offeman, R.E. Preparation of Graphitic Oxide. *J. Am. Chem. Soc.* **1958**, *80*, 1339. [[CrossRef](#)]
33. Stankovich, S.; Dikin, D.A.; Piner, R.D.; Kohlhaas, K.A.; Kleinhammes, A.; Jia, Y.; Wu, Y.; Nguyen, S.B.T.; Ruoff, R.S. Synthesis of graphene-based nanosheets via chemical reduction of exfoliated graphite oxide. *Carbon* **2007**, *45*, 1558–1565. [[CrossRef](#)]
34. Zhang, H.; Wang, S.; Lin, Y.; Feng, M.; Wu, Q. Stability, thermal conductivity, and rheological properties of controlled reduced graphene oxide dispersed nanofluids. *Appl. Therm. Eng.* **2017**, *119*, 132–139. [[CrossRef](#)]
35. Wang, X.Q.; Mujumdar, A.S. A review on nanofluids—Part II: Experiments and applications. *Brazilian J. Chem. Eng.* **2008**, *25*, 631–648. [[CrossRef](#)]
36. Ettefaghi, E.; Ghobadian, B.; Rashidi, A.; Najafi, G.; Khoshtaghaza, M.H.; Pourhashem, S. Preparation and investigation of the heat transfer properties of a novel nanofluid based on graphene quantum dots. *Energy Convers. Manag.* **2017**, *153*, 215–223. [[CrossRef](#)]
37. Hernandez, Y.; Nicolosi, V.; Lotya, M.; Blighe, F.M.; Sun, Z.; De, S.; McGovern, I.T.; Holland, B.; Byrne, M.; Gun'ko, Y.K.; et al. High-yield production of graphene by liquid-phase exfoliation of graphite. *Nat. Nanotechnol.* **2008**, *3*, 563–568. [[CrossRef](#)]

38. Sarsam, W.S.; Kazi, S.N.; Badarudin, A. Thermal performance of a flat-plate solar collector using aqueous colloidal dispersions of graphene nanoplatelets with different specific surface areas. *Appl. Therm. Eng.* **2020**, *172*, 115142. [[CrossRef](#)]
39. Wang, Z.; Wu, Z.; Han, F.; Wadsö, L.; Sundén, B. Experimental comparative evaluation of a graphene nanofluid coolant in miniature plate heat exchanger. *Int. J. Therm. Sci.* **2018**, *130*, 148–156. [[CrossRef](#)]
40. Haque, A.K.M.M.; Kim, S.; Kim, J.; Noh, J.; Huh, S.; Choi, B.; Chung, H.; Jeong, H. Surface Modification of Graphene Nanoparticles by Acid Treatment and Grinding Process. *J. Nanosci. Nanotechnol.* **2017**, *18*, 645–650. [[CrossRef](#)]
41. Kim, S.; Song, H.; Yu, K.; Tserengombo, B.; Choi, S.H.; Chung, H.; Kim, J.; Jeong, H. Comparison of CFD simulations to experiment for heat transfer characteristics with aqueous Al₂O₃ nanofluid in heat exchanger tube. *Int. Commun. Heat Mass Transf.* **2018**, *95*, 123–131. [[CrossRef](#)]
42. Shahrul, I.M.; Mahbulbul, I.M.; Saidur, R.; Sabri, M.F.M. Experimental investigation on Al₂O₃-W, SiO₂-W and ZnO-W nanofluids and their application in a shell and tube heat exchanger. *Int. J. Heat Mass Transf.* **2016**, *97*, 547–558. [[CrossRef](#)]
43. Wang, N.; Xu, G.; Li, S.; Zhang, X. Thermal Properties and Solar Collection Characteristics of Oil-based Nanofluids with Low Graphene Concentration. *Energy Procedia* **2017**, *105*, 194–199. [[CrossRef](#)]
44. Goodarzi, M.; Kherbeet, A.S.; Afrand, M.; Sadeghinezhad, E.; Mehrali, M.; Zahedi, P.; Wongwises, S.; Dahari, M. Investigation of heat transfer performance and friction factor of a counter-flow double-pipe heat exchanger using nitrogen-doped, graphene-based nanofluids. *Int. Commun. Heat Mass Transf.* **2016**, *76*, 16–23. [[CrossRef](#)]
45. Huu-Quan, D.; Mohammad Rostami, A.; Shokri Rad, M.; Izadi, M.; Hajjar, A.; Xiong, Q. 3D numerical investigation of turbulent forced convection in a double-pipe heat exchanger with flat inner pipe. *Appl. Therm. Eng.* **2021**, *182*, 116106. [[CrossRef](#)]
46. Wang, Q.; Song, Z.; Zheng, Y.; Yin, Y.; Liu, L.; Wang, H.; Yao, J. Coupled convection heat transfer of water in a double pipe heat exchanger at supercritical pressures: An experimental research. *Appl. Therm. Eng.* **2019**, *159*, 113962. [[CrossRef](#)]
47. Omidi, M.; Farhadi, M.; Jafari, M. A comprehensive review on double pipe heat exchangers. *Appl. Therm. Eng.* **2017**, *110*, 1075–1090. [[CrossRef](#)]
48. Xuana, Y.; Roetzel, W. Conceptions for heat transfer correlation of nanofluids. *Int. J. Heat Mass Transf.* **2000**, *43*, 3701–3707. [[CrossRef](#)]
49. Pak, B.C.; Cho, Y.I. Hydrodynamic and Heat Transfer Study of Dispersed Fluids With Submicron Metallic Oxide. *Exp. Heat Transf. Int. J.* **1998**, *11*, 151–170. [[CrossRef](#)]
50. Qiu, L.; Wang, X.; Su, G.; Tang, D.; Zheng, X.; Zhu, J.; Wang, Z.; Norris, P.M.; Bradford, P.D.; Zhu, Y. Remarkably enhanced thermal transport based on a flexible horizontally-aligned carbon nanotube array film. *Sci. Rep.* **2016**, *6*, 21014. [[CrossRef](#)]
51. Yarmand, H.; Gharekhani, S.; Shirazi, S.F.S.; Goodarzi, M.; Amiri, A.; Sarsam, W.S.; Alehashem, M.S.; Dahari, M.; Kazi, S.N. Study of synthesis, stability and thermo-physical properties of graphene nanoplatelet/platinum hybrid nanofluid. *Int. Commun. Heat Mass Transf.* **2016**, *77*, 15–21. [[CrossRef](#)]
52. Amiri, A.; Shanbedi, M.; Yarmand, H.; Arzani, H.K.; Gharekhani, S.; Montazer, E.; Sadri, R.; Sarsam, W.; Chew, B.T.; Kazi, S.N. Laminar convective heat transfer of hexylamine-treated MWCNTs-based turbine oil nanofluid. *Energy Convers. Manag.* **2015**, *105*, 355–367. [[CrossRef](#)]
53. Rabiei, S.; Khosravi, R.; Bahiraei, M.; Razi, M.; Ahmadian Hosseini, A. Thermal and hydraulic characteristics of a hybrid nanofluid containing graphene sheets decorated with platinum through a new wavy cylindrical microchannel. *Appl. Therm. Eng.* **2020**, *181*, 115981. [[CrossRef](#)]
54. Halim, M.A.; Mohd, N.; Nasir, M.N.; Dahalan, M.N. The Evaluation of k- ϵ and k- ω Turbulence Models in Modelling Flows and Performance of S-shaped Diffuser. *Int. J. Automot. Mech. Eng.* **2018**, *15*, 2013–2015.
55. Ghanbari, S.; Javaherdeh, K. Thermal performance enhancement in perforated baffled annuli by nanoporous graphene non-Newtonian nanofluid. *Appl. Therm. Eng.* **2020**, *167*, 114719. [[CrossRef](#)]
56. Saeedan, M.; Solaimany Nazar, A.R.; Abbasi, Y.; Karimi, R. CFD Investigation and neutral network modeling of heat transfer and pressure drop of nanofluids in double pipe helically baffled heat exchanger with a 3-D finned tube. *Appl. Therm. Eng.* **2016**, *100*, 721–729. [[CrossRef](#)]
57. Arzani, H.K.; Amiri, A.; Kazi, S.N.; Chew, B.T.; Badarudin, A. Experimental and numerical investigation of thermophysical properties, heat transfer and pressure drop of covalent and noncovalent functionalized graphene nanoplatelet-based water nanofluids in an annular heat exchanger. *Int. Commun. Heat Mass Transf.* **2015**, *68*, 267–275. [[CrossRef](#)]
58. Sadeghinezhad, E.; Togun, H.; Mehrali, M.; Sadeghi Nejad, P.; Tahan Latibari, S.; Abdulrazzaq, T.; Kazi, S.N.; Metselaar, H.S.C. An experimental and numerical investigation of heat transfer enhancement for graphene nanoplatelets nanofluids in turbulent flow conditions. *Int. J. Heat Mass Transf.* **2015**, *81*, 41–51. [[CrossRef](#)]
59. Ranjbarzadeh, R.; Karimipour, A.; Afrand, M.; Isfahani, A.H.M.; Shirneshan, A. Empirical analysis of heat transfer and friction factor of water/graphene oxide nanofluid flow in turbulent regime through an isothermal pipe. *Appl. Therm. Eng.* **2017**, *126*, 538–547. [[CrossRef](#)]
60. Khairul, M.A.; Alim, M.A.; Mahbulbul, I.M.; Saidur, R.; Hepbasli, A.; Hossain, A. Heat transfer performance and exergy analyses of a corrugated plate heat exchanger using metal oxide nanofluids. *Int. Commun. Heat Mass Transf.* **2014**, *50*, 8–14. [[CrossRef](#)]
61. Mohammed, H.A.; Narrein, K. Thermal and hydraulic characteristics of nanofluid flow in a helically coiled tube heat exchanger. *Int. Commun. Heat Mass Transf.* **2012**, *39*, 1375–1383. [[CrossRef](#)]
62. Lima, A.A.; Ochoa, A.A.; Da Costa, J.A.; Henriquez, J. CFD simulation of heat and mass transfer in an absorber that uses the pair ammonia/water as a working fluid. *Int. J. Refrig.* **2019**, *98*, 514–525. [[CrossRef](#)]

63. Ochoa, A.A.V.; Dutra, J.C.C.; Henríquez, J.R.G.; Dos Santos, C.A.C. Dynamic study of a single effect absorption chiller using the pair LiBr/H₂O. *Energy Convers. Manag.* **2016**, *108*, 30–42. [[CrossRef](#)]
64. Incropera, F.P.; DeWitt, D.P.; Bergman, T.L.; Lavine, A.S. *Fundamentals of Heat and Mass Transfer*; John Wiley & Sons: Hoboken, NJ, USA, 2007; Volume 108, ISBN 9780471457282.
65. Gnielinski, V. New Equations for Heat and Mass Transfer in Turbulent Pipe and Channel Flow. *Int. Chem. Eng.* **1976**, *16*, 359–368.
66. Petukhov, B.S. Heat Transfer and Friction in Turbulent Pipe Flow with Variable Physical Properties. *Adv. Heat Transf.* **1970**, *6*, 503–564. [[CrossRef](#)]
67. Sadri, R.; Mallah, A.R.; Hosseini, M.; Ahmadi, G.; Kazi, S.N.; Dabbagh, A.; Yeong, C.H.; Ahmad, R.; Yaakup, N.A. CFD modeling of turbulent convection heat transfer of nanofluids containing green functionalized graphene nanoplatelets flowing in a horizontal tube: Comparison with experimental data. *J. Mol. Liq.* **2018**, *269*, 152–159. [[CrossRef](#)]
68. Sadri, R.; Hosseini, M.; Kazi, S.N.; Bagheri, S.; Abdelrazek, A.H.; Ahmadi, G.; Zubir, N.; Ahmad, R.; Abidin, N.I.Z. A facile, bio-based, novel approach for synthesis of covalently functionalized graphene nanoplatelet nano-coolants toward improved thermo-physical and heat transfer properties. *J. Colloid Interface Sci.* **2018**, *509*, 140–152. [[CrossRef](#)]
69. Han, D.; He, W.F.; Asif, F.Z. Experimental study of heat transfer enhancement using nanofluid in double tube heat exchanger. *Energy Procedia* **2017**, *142*, 2547–2553. [[CrossRef](#)]
70. Palanisamy, K.; Kumar, P.C.M. Heat transfer enhancement and pressure drop analysis of a cone helical coiled tube heat exchanger using MWCNT/water nanofluid. *J. Appl. Fluid Mech.* **2017**, *10*, 7–13. [[CrossRef](#)]
71. Cengel, Y.; Ghajar, A. *Heat and Mass Transfer: Fundamentals and Applications*, 5th ed.; McGraw Hill: New York, NY, USA, 2014; ISBN 2013206534.
72. Kumar, V.; Tiwari, A.K.; Ghosh, S.K. Effect of variable spacing on performance of plate heat exchanger using nanofluids. *Energy* **2016**, *114*, 1107–1119. [[CrossRef](#)]
73. Hosseini, M.; Abdelrazek, A.H.; Sadri, R.; Mallah, A.R.; Kazi, S.N.; Chew, B.T.; Rozali, S.; Yusoff, N. Numerical study of turbulent heat transfer of nanofluids containing eco-friendly treated carbon nanotubes through a concentric annular heat exchanger. *Int. J. Heat Mass Transf.* **2018**, *127*, 403–412. [[CrossRef](#)]
74. Blasius, H. *The Boundary Layers in Fluids with Little Friction*; No. 1256; National Advisory Committee for Aeronautics: Edwards, CA, USA, 1907; pp. 1–37.
75. Andrade, L.; Carvalho, J.d.A. Análise da equação de Swamee-Jain para cálculo do fator de atrito. *Rev. Bras. Eng. Agrícola Ambient.* **2001**, *5*, 554–557. [[CrossRef](#)]
76. Colebrook, C.F.; Blench, T.; Chatley, H.; Essex, E.H.; Finnicome, J.R.; Lacey, G.; Williamson, J.; Macdonald, G.G. Correspondence. Turbulent Flow in Pipes, With Particular Reference To the Transition Region between the Smooth and Rough Pipe Laws. (Includes Plates). *J. Inst. Civ. Eng.* **1939**, *12*, 393–422. [[CrossRef](#)]
77. Sajjad, M.; Kamran, M.S.; Shaukat, R.; Zeinelabdeen, M.I.M. Numerical investigation of laminar convective heat transfer of graphene oxide/ethylene glycol-water nanofluids in a horizontal tube. *Eng. Sci. Technol. Int. J.* **2018**, *21*, 727–735. [[CrossRef](#)]
78. Wang, S.; Xiao, J.; Ye, S.; Song, C.; Wen, J. Numerical investigation on pre-heating of coal water slurry in shell-and-tube heat exchangers with fold helical baffles. *Int. J. Heat Mass Transf.* **2018**, *126*, 1347–1355. [[CrossRef](#)]
79. Khajeh Arzani, H.; Amiri, A.; Arzani, H.K.; Rozali, S.B.; Kazi, S.N.; Badarudin, A. Toward improved heat transfer performance of annular heat exchangers with water/ethylene glycol-based nanofluids containing graphene nanoplatelets. *J. Therm. Anal. Calorim.* **2016**, *126*, 1427–1436. [[CrossRef](#)]
80. Selvam, C.; Balaji, T.; Mohan Lal, D.; Harish, S. Convective heat transfer coefficient and pressure drop of water-ethylene glycol mixture with graphene nanoplatelets. *Exp. Therm. Fluid Sci.* **2017**, *80*, 67–76. [[CrossRef](#)]
81. Bahiraei, M.; Kiani Salmi, H.; Safaei, M.R. Effect of employing a new biological nanofluid containing functionalized graphene nanoplatelets on thermal and hydraulic characteristics of a spiral heat exchanger. *Energy Convers. Manag.* **2019**, *180*, 72–82. [[CrossRef](#)]
82. Bahiraei, M.; Mazaheri, N.; Rizehvandi, A. Application of a hybrid nanofluid containing graphene nanoplatelet–platinum composite powder in a triple-tube heat exchanger equipped with inserted ribs. *Appl. Therm. Eng.* **2019**, *149*, 588–601. [[CrossRef](#)]
83. Ravi Kumar, N.T.; Bhramara, P.; Sundar, L.S.; Singh, M.K.; Sousa, A.C.M. Heat transfer, friction factor and effectiveness of Fe₃O₄ nanofluid flow in an inner tube of double pipe U-bend heat exchanger with and without longitudinal strip inserts. *Exp. Therm. Fluid Sci.* **2017**, *85*, 331–343. [[CrossRef](#)]

Disclaimer/Publisher’s Note: The statements, opinions and data contained in all publications are solely those of the individual author(s) and contributor(s) and not of MDPI and/or the editor(s). MDPI and/or the editor(s) disclaim responsibility for any injury to people or property resulting from any ideas, methods, instructions or products referred to in the content.